

IISc THESES ABSTRACTS

Thesis Abstract (Ph. D.)

Analysis of the acoustic wave propagation in variable area flow ducts and anechoic linings by V. Easwaran

Research supervisor: M. L. Munjal

Department: Mechanical Engineering

1. Introduction

In the present thesis, the use of analytical and finite-element tools to analyze certain practical acoustic wave propagation problems has been demonstrated, bridging in the process some of the lacunae that exist in the literature. The analysis is restricted primarily to the frequency domain, and also to linear systems.

The problems investigated in this thesis are: variable area flow ducts, acoustically absorptive wedges and resonator-type absorptive linings (Alberich linings). While the variable area flow ducts have been analyzed analytically, the wedges and Alberich linings have been analyzed by means of finite-element methods.

2. Variable area flow ducts

Analytical solutions for a plane wave propagation have been available for uniform area ducts with moving medium and variable area ducts with stationary medium. Often, variable area ducts can be found in flow duct systems such as air-conditioning systems, gas distribution systems, expansion chambers, intake and exhaust ductwork of compressors, piston engines, fans and in the electro-pneumatic transducers. In this thesis, a generalized velocity potential equation characterizing the wave propagation in variable area ducts, in the presence of an almost incompressible mean flow, has been derived. Closed-form analytical solutions of this equation have been obtained for the following duct shapes: conical, exponential, hyperbolic and parabolic. Self-consistent expressions for the transfer matrix, the impedance matrix and the scattering matrix of these ducts have been derived. Also, expressions have been derived for the transmission loss of isolated conical and exponential ducts, as well as for expansion chambers involving these ducts. It has also been shown in the process that a suitable selection of parameters of the hyperbolic duct yields solutions for duct shapes such as conical, exponential, catenoidal, sine and cosine. Comparison has also been made with the relevant experimental results available in the literature¹. It has been observed that mean flow introduces out-of-phase components in the transfer matrix components. The corresponding in-phase components have been observed to be affected only marginally, because of flow. Also, the effect of mean flow on the transmission loss of isolated variable area ducts as well as expansion chambers involving these ducts has been found to be marginal. Expansion chambers with variable area elements have been observed to be inferior to the corresponding simple expansion chambers from the point of view of noise abatement.

A segmentation method has been suggested for variable area shapes for which exact solutions could not be obtained. This method involves discretizing the variable area duct into small segments so that the mean flow in each of these segments can be assumed to be constant. Such a segmentation method also accounts for compressible mean flow. In the process, incorrectness in the use of segmentation method elsewhere in the literature^{1,2} in the presence of a mean flow has been highlighted. The incorrectness has been shown to stem from the fact that the acoustic pressure and the acoustic mass velocity are not conserved in the presence of flow, across the notional discontinuity between two adjoining segments. A discontinuity transfer matrix has been derived, incorporating the effect of compressible mean flow. This transfer matrix has been shown to remedy the afore-mentioned incorrectness.

The analytical investigation has been extended to the study of variable-area extended inlet/outlet expansion chambers. Governing equation for wave motion in the variable area annulus formed by an outer uniform duct and

an inner (coaxial) variable area duct has been derived and has been solved analytically for three different variable area shapes: conical, exponential and parabolic. While power series method has been used to analyze conical as well as exponential duct annulus, the parabolic duct annulus has been analyzed using the Bessel function expansions. Also, the transfer matrix and the impedance matrix of annulus of such variable area annuli have been derived. It has been found that expansion chambers with variable area extended inlet/outlet are inferior to expansion chambers with constant area elements, from the point of view of noise abatement.

3. Inter-relationships between the impedance matrix, transfer matrix and the scattering matrix

Some interesting properties were observed in the transfer matrix, the impedance matrix and the scattering matrix of variable area ducts. As such, relationships between the impedance matrix, the transfer matrix and the scattering matrix have been established comprehensively for a general dynamical system characterized by a finite number of degrees of freedom. The properties of such matrices when the system is symmetric, reciprocal and conservative have been studied. It has been shown that the determinant of the transfer matrix of a reciprocal system is ± 1 . Similarly, the transfer matrix of a symmetrical system has been shown to be involuntary. The impedance matrix of a conservative system has been shown to be skew-Hermitian. It has also been shown that when the system is conservative and reciprocal, the impedance matrix is purely imaginary. In the corresponding transfer matrix, submatrices T_a and T_d become real and the submatrices, T_b and T_c , become purely imaginary. In addition, cascading of the symmetrical, reciprocal and conservative systems has been studied.

4. Analysis of wedges

Another variable area situation exists in the case of wedges used in anechoic chambers, with the significant difference that there are two media (the wedge material and air) alternating with each other, forming thus a coupled problem. Usually, these wedges are tested for their absorptive and reflective properties in an impedance tube under normal incidence. In the present investigation this problem has been analyzed by making use of the finite-element method, as it defines analytical solution. In this connection, a theoretical model based on the bulk reaction concept has been presented for modelling the behaviour of wedges in the impedance tube. Two different types of wedges have been analyzed: rectangular wedge, and conical wedge. Theoretical predictions have been validated against the experimental results reported in other publications³. A computer program has also been developed based on the finite-element method to analyze the reflection characteristics of wedges. These computations have been performed on a desktop computer (on a PC environment). In fact, the computer program developed has been used to design the wedges for the anechoic chamber to be constructed by TELCO, at its Engineering Research Centre in Pune, India. Parametric studies have been made using the computer program in order to evolve design curves for foam materials. The effect of using different materials for wedges has been highlighted. The wedge length, the flow resistivity and the air gap, emerge as most important design parameters. Conical wedges have also been shown to be generally inferior to the corresponding rectangular wedges.

5. Analysis of Alberich linings

Wedges are normally used only for in-air anechoic applications. They cannot, however, be used for anechoic underwater applications like submarines, which need to be protected against acoustic detection by active sonar of alien underwater vehicles. Alberich linings have been found to be ideal for such applications. These linings are multi-layered linings made of viscoelastic material consisting of a perforated layer sandwiched between a cover layer and a base layer (or the hull of the underwater vehicle). These coatings are normally intended for use on surfaces which are usually perpendicular to either the target, the transmitter or the receiver of an active sonar. As in the case of wedges, a finite-element approach has been used to analyze such linings, as closed-form analytical solutions are difficult to obtain, if not impossible. A novel finite-element scheme for analyzing the reflection characteristics of resonant sound absorber linings has been presented in this thesis. It has been shown that the fluid can be modeled with equivalent Lamé constants, as an elastic medium. Modal decomposition technique used elsewhere in the literature, in the fluid, has been replaced by one in which the corresponding impedance boundary conditions are specified. This results in an overall matrix which is symmetric, sparse and banded instead of a nearly fully populated matrix. Also, a quarter symmetry feature within the periodic unit cell has been exploited, resulting in substantial savings in pre-computation effort, core memory and the computation time and hence the costs. The

finite-element scheme proposed has also been validated with the experimental results presented elsewhere in the literature⁴. A computer program has been developed based on the theoretical model presented in this thesis as a part of the ongoing project with the Department of Electronics (DOE), Government of India, on the development of stealth linings for underwater vehicles. Here again, the computer program has been used to generate design curves with a variety of geometrical and material parameters for air closure as well as water closure. The diameter of the perforations, the Young's modulus of elasticity of the viscoelastic material and its loss factor, and the type of closure: water or air, have been found to have a dominant effect on the performance of these linings.

References

1. LUNG, T. Y. AND DOIGE, A. G. A time-averaging transient testing method for acoustic properties of piping systems and muffers with flow, *J. Acoust. Soc. Am.*, 1983, 73, 867-876.
2. MILES, J. H. Acoustic transmission of a variable area duct or a nozzle carrying a compressible subsonic flow, *J. Acoust. Soc. Am.*, 1981, 69, 1577-1586.
3. KOIDAN, W., HRUSKA, G. R. AND PICKETT, A. Wedge design for National Bureau of Standards anechoic chamber, *J. Acoust. Soc. Am.*, 1971, 52, 1071-1076.
4. HENNION, A. C. AND DECARPIGNY, J. N. Analysis of the scattering of a plane acoustic wave by a doubly periodic elastic structure using the finite element method: Application to Alberich anechoic coatings, *J. Acoust. Soc. Am.*, 1991, 90, 3356-3367.

Thesis Abstract (Ph. D.)

Modelling of drop breakage in stirred vessels by D. K. Rajeev Nambiar

Research supervisors: K. S. Gandhi and T. R. Das

Department: Chemical Engineering

1. Introduction

The stirred vessel finds diverse applications in the chemical process industry. It is a very convenient device for contacting two immiscible liquid phases to effect mass transfer of a desired solute from one phase to the other. The attractiveness of the stirred vessel stems in part from the large interfacial area obtained by maintaining one of the phases as droplets in the other, continuous, phase. Turbulent conditions are usually required to maximize the effectiveness of the unit. The accurate estimation of transfer rates constitutes an important design input. The dispersed phase droplet population exhibits a distribution of size, and averaging without taking account of this polydispersity can result in wrong estimates of transfer rates.

The population balance equation¹(PBE) provides the analytical tool for mathematical analysis of such systems. It is a statement of number balance that takes explicit account of the phenomena of breakage and coalescence of the dispersed phase droplets. The present work focuses on drop breakage is provided by specifying $\Gamma(v')$, the rate at which drops of a given size v' break, $\nu(v')$, the mean number of daughter droplets resulting from such a breakage and $\beta(v, v')$, their probable sizes. This mathematical description of drop breakage in terms $\Gamma(v)$, $\nu(v)$ and $\beta(v, v')$ enters the population balance equation for the pure breakage problem. The PBE can then be solved analytically or numerically to obtain the transient and steady-state drop size distributions.

2. Development of the model

It is known that for a given intensity of turbulence prevailing in the vessel, there always exists a critical drop size, d_{max} , below which the drops are stable to the turbulence, *i.e.*, they do not fragment under the action of the pressure fluctuations that characterize turbulent flow². Even when coalescence is negligible, therefore, a steady state is reached when all the drops in the systems have broken down to sizes below d_{max} . There are several models in the

literature that estimate this maximum stable drop diameter given the operating conditions and the physical properties of the system. There are however very few that discuss how the drop size is distributed in the range below d_{max} . The present work addresses this problem. To this end, it has been attempted to derive, from a simple one-dimensional model of drop breakage, expressions for both the breakage frequency and the daughter droplet size distribution.

The deformation and breakage of the drop is driven by pressure fluctuations across points on the drop surface. The dynamic pressure fluctuations responsible for the deformation of the drop may be viewed as resulting from its interaction with turbulent eddies of varying size. It has been customary to use Kolmogorov's theory to describe the energy characteristics of the eddies. The earlier work in the field on prediction of the maximum stable drop diameter, d_{max} , considered the interaction of a drop with eddies of the size of the drop diameter. Eddies larger than the drop merely convect it along with the mean flow while eddies smaller than it have lower energy and shorter lifetimes and need not therefore be considered in any analysis that seeks only to predict d_{max} . Since the present work seeks to predict the entire drop size distribution, the fragmentation of drops larger than d_{max} is of interest. Such drops can break asymmetrically³ and therefore necessitate an analysis different from that employed for d_{max} prediction where the drop is assumed to split into two equal daughter droplets. In this work, such asymmetric fragmentation of the drop is modelled as resulting from the interaction of the drop with eddies of size smaller than the drop diameter.

The deformation of the drop under the action of an eddy is opposed by the drop viscosity and the interfacial tension. A Voigt element comprising a spring and dashpot in parallel therefore provides the simplest description of a deforming drop⁴. For symmetric breakage of the drop, the ratio of the interfacial tension to the drop diameter is taken as an estimate of the restoring stress represented by the spring. Unequal breakage produces daughter droplets with a smaller total surface area than does equal breakage. Hence in this work the above estimate of the restoring stress due to interfacial tension is modified in proportion to the asymmetry of the breakage. Furthermore, interfacial tension does not resist the drop deformation all the way and is even known to aid the formation of daughter droplets at incipient breakage. In the present model this feature is captured by introducing a nonlinearity in the constitutive equation for the restoring action of the spring. The entire deformation and breakage of the drop has to occur within a time span of the mean lifetime of the eddy. This places a lower limit on the size of the eddy that can break the drop. The upper limit is set by considerations of drop convection with the mean flow. There is thus, for each drop that can be broken in the turbulent flow field, a range of eddies that can cause it to fragment. This leads to an equivalent description of d_{max} as that drop diameter for which this range of eddy sizes shrinks to a single point.

Analytical expressions for both the breakage frequency and the daughter droplet size distribution follow from an examination of the pattern of interaction of the drop with the various eddies in the stirred vessel. Since it is known that breakage predominates in only a small region of the stirred vessel in the immediate vicinity of the impeller, the stirred vessel is divided into a breakage zone and a circulation zone. The drop cycles alternately between these two zones. Drop-eddy interactions are presumed to be negligible in the circulation zone in view of the comparatively lower turbulence intensity levels that characterize this zone. An eddy size distribution is assumed in the breakage zone to take account the stochastic nature of the interaction of eddies with the drop. The life history of a typical drop in the stirred vessel is then considered and is seen to comprise ineffective interactions with small eddies interspersed with periods of circulation. It is possible to estimate the expected survival time of a drop in the stirred vessel before it loses its identity through fragmentation. The reciprocal of this expected survival time may be taken as the breakage frequency of the drop. The daughter droplet distribution is related to the eddy size distribution and is obtained by estimating the probability that the drop fragmentation eventually occurred owing to the interaction of the drop with a specific eddy.

3. Results and discussion

The population balance equation for the pure breakage problem is solved numerically with the above expressions for the breakage frequency and the daughter droplet distribution, and both transient and steady-state drop size distributions are obtained. Since the steady state is characterized by all the drops in the system being of size smaller than d_{max} , an analytical solution of the system of ODEs describing the discretized PBE can be used to obtain the steady-state drop size distributions. The size distributions predicted by the model are compared with the

available experimental data. Except for dispersed phases of very high velocity or when the interfacial tension between the dispersed and the continuous phases is very low, the model predicts the experimental data reasonably well. It also generalizes naturally to dispersed phases of non-Newtonian flow behaviour. The extensions for Bingham plastics, power law fluids and mildly viscoelastic fluids as dispersed phases have been considered.

4. Some extensions

In the high viscosity–low interfacial tension cases where the present model does not predict the size distribution correctly, the models available in the literature for d_{max} prediction alone are also found wanting. Recent work by Kumar *et al.*⁵ has indicated the possibility that in such cases the drop may not entirely relax back to its spherical shape in the circulation zone in the event of surviving an eddy in the breakage zone. Subsequent eddy interactions can then build on this residual deformation. Based on the above idea, a multistage extension of drop breakage model has been developed. The resulting analytical expressions for the breakage frequency and the daughter droplet distribution are fairly complex. A simulation approach has therefore been employed to obtain expressions for these and also the steady-state drop size distributions. While the multistage model yields results entirely consistent with the earlier single stage model for systems of moderate viscosity and interfacial tension, it also predicts the drop size distributions for high dispersed phase viscosity–low interfacial tension systems much more correctly.

References

1. HULBURT, H. M. AND KATZ, S. Some problems in particulate technology—A statistical mechanical formulation, *Chem. Engng Sci.*, 1964, 19, 555–574.
2. HINZE, J. O. Fundamentals of the hydrodynamic mechanism of splitting in dispersion processes, *AIChEJ.*, 1955, 1, 289–295.
3. NAMBIAR, D. K. R., KUMAR, R., DAS, T. R. AND GANDHI, K. S. A new model for the breakage frequency of drops in turbulent stirred dispersions, *Chem. Engng Sci.*, 1992, 47, 2989–3002.
4. LAGISETTY, J. S., DAS, P. K., KUMAR, R. AND GANDHI, K. S. Breakage of viscous and non-Newtonian drops in stirred dispersions, *Chem. Engng Sci.*, 1992, 41, 65–72.
5. KUMAR, S., KUMAR, R. AND GANDHI, K. S. A multi-stage model for drop breakage in stirred vessels, *Chem. Engng Sci.*, 1992, 47, 971–980.

Thesis Abstract (Ph. D.)

Studies on membrane formation and diffusion coupled enzymatic reaction in semipermeable microcapsules by G. Aruna

Research supervisor: M. S. Murthy

Department: Chemical Engineering

1. Introduction

Liquid-filled semipermeable nylon microcapsules find extensive applications in controlled release of substances, in bioreactors for enzyme immobilization and affinity purification of low molecular weight, biologically active agents by entrapped ligands. For any given application, the transfer rates of substances across these microcapsules depend on factors like a) the size of the capsules, b) the membrane characteristics, and c) the hydrodynamic characteristics of the external liquid medium. When the first and the third conditions are fixed, membrane characteristics greatly influence the rates of material transfer across these microcapsules; hence, a knowledge of thickness, permeability and pore-size distribution of the membrane is essential. In the present investigation it is intended to prepare the microcapsules with known membrane characteristics, to characterize the membrane based on its permeability to different solute molecules and to study the application of these microcapsules in biochemical reactors for enzyme immobilization.

2. Preparation of microcapsules with desired membrane characteristics

Microcapsules are prepared by the method of interfacial polymerization. Droplets of HMDA (hexamethylenediamine) in aqueous phases and are dispersed into an organic phase containing SBC (sebacoyl chloride). *In situ* polymerization takes place at the interface giving rise to a thin polymer membrane around the aqueous droplet. Initial characteristics of the membrane depend on reaction condition like concentration of the monomers, temperature of the reaction and time. Further growth of the membrane depends on the mass transfer rate of the HMDA from the aqueous droplet through the growing membrane to the reaction site. A model was proposed based on moving boundary-type problems to explain the phenomenon of membrane formation.

The method of preparation of microcapsules was modified from the procedure available in literature¹⁻² so as to monitor the membrane growth rate. A model was proposed to predict the rate of growth of the membrane and the experimental values of membrane thickness (measured by SEM technique) compared well with model predictions. A satisfactory semi-empirical expression was developed to correlate the effective diffusivity of HMDA through the growing membrane, in terms of its conversion.

The model predictions compared well with experimental data. From eqn 1 it is said that the membrane thickness at any time depends on the initial concentration of HMDA, the time of exposure to organic medium, and the temperature of the reaction. The process offers the flexibility of parameter adjustment to prepare microcapsules with desired membrane thicknesses.

3. Characterization of membranes of microcapsules

The membrane was characterized on the basis of its permeability or effective diffusivity to the diffusing solute molecule. The transient diffusion experiments were carried out by encapsulating different molecular weight substances to find the cut-off point of the molecular weight. The release of various encapsulated substances through the microcapsules was monitored experimentally and the rates of release were used to estimate the membrane permeabilities. An unsteady state transport model was used to predict independently the membrane permeabilities. The model incorporates a modified fictitious Sherwood group to account for the overall mass transfer resistance which gives the picture of the resistance encountered by the diffusing molecule from the capsule into the environment. The observed and the predicted effective diffusivity values matched well. These were also compared with modified correlations accounting for steric hindrance and hydrodynamic drag exerted on the diffusing molecular species.

4. Application of microcapsules in biotechnology

The application of these microcapsules in biochemical reactors was demonstrated by using urea-urease as a test system. The enzyme urease was encapsulated, and the urea decomposition rates were studied with both soluble and immobilized enzyme systems. Kinetic constants were calculated in both the cases. The measured rates of reaction were compared with the predicted ones and the effectiveness factors were calculated. A theoretical expression was developed to predict the diffusion-coupled enzymatic reaction rates a priori when there is information on the membrane characteristics and homogeneous kinetics of the enzyme. Alternatively, to cross-check the above results another theoretical expression was developed, which gave the membrane characteristics when the soluble and immobilized enzyme reaction rates are known. The second expression incorporates a fictitious Sherwood group similar to a pure diffusion process (described in Section 3). It was found that in both the cases the fictitious Sherwood group was found to match exactly showing the accuracy of the results obtained for a pure diffusion process.

When the activity of the enzyme was measured before and after immobilization, no change was observed in the activity. When the kinetic parameters, the maximum rate of reaction and Michaelis constant were compared, there was a reduction in the maximum rate of reaction but no change was observed in the value of Michaelis constant, showing that the reduction in rates was due to the presence of the membrane, and not due to structural changes in enzyme molecules which are associated with other methods of immobilization³.

5. Conclusions

The following conclusions were drawn from the present study.

1. Semipermeable microcapsule capsules could be prepared with desired membrane characteristics by adjusting the reaction conditions.
2. The membranes were successfully characterized based on the effective diffusivity/permeability to various solute molecules.
3. These capsules were used in biochemical reactors for the immobilization of enzymes. When data on the homogeneous enzymatic reaction and membrane characteristics is available, the diffusion-coupled enzymatic rates can be predicted a priori. Alternatively, if the immobilized enzyme reaction rates are known, from a knowledge of homogeneous kinetic rates, the membrane characteristics rates could be determined accurately.
4. The advantage of this method of enzyme immobilization is that the enzyme is that only insolubilized and not immobilized as evident from the activity measurements and the kinetic constants. There was no change in the Michaelis constant (which is an intrinsic parameter) showing that no conformational changes occurred in the enzyme molecule during the process of immobilization.
5. The above study is of great help, as it offers the uniqueness of cross-checking the results obtained either for pure diffusion system or for a diffusion-coupled reaction system.
6. Above all, the process offers the flexibility in choosing the conditions of encapsulation to obtain the desired release rates/reaction rates as the case may be.
7. The investigation carried out broadly revealed the possibility of designing microcapsules with desired membrane thicknesses and characteristics specific to the intended application. Such a skill is crucial not only in the design of microcapsules for a controlled release system or for enzyme immobilization, but also to protect a biologically active substance from the environment for its protection and prolonged usage.

References

1. CHANG, T. M. S.,
MACINTOSH, F. C.
AND MASON, S. G. Semipermeable aqueous microcapsules. Preparation and properties, *Can. J. Physiol. Pharmacol.*, 1966, 44, 115-128.
2. MORGON, P. W. *Condensation polymers: by interfacial and solution methods*, 1965, Interscience.
3. RONY, P. R. Multiphase catalysis. II Hollow fiber catalysts, *Biotech. Bioengng.*, 1971, 13, 431-447.

Thesis Abstract (M. Sc. (Engng))

Stability and performance analysis of some multiple access and mobile cellular communications networks by B. V. Prathima

Research supervisor: Vinod Sharma

Department: Electrical Engineering

1. Introduction

In this thesis we study the stability and performance of some communication networks. The thesis has two parts. In the first, we study a cellular mobile communications system and in the second, we develop an access scheme for satellite communication networks.

2. Mobile cellular communication system

2.1. Introduction

In the cellular radio system, the entire geographical area in which service is provided is divided into smaller regions referred to as 'cells'. Each cell has a base station and has a limited number of frequency channels to be used by the mobiles lying in its area. The mobiles move randomly and are allowed to move from one cell to another. Mobile units which initiate a call will be allocated a frequency channel if there is at least one channel free in the cell in which the mobile unit is located. When the mobile moves out of the cell into another cell the call is transferred to the base station of the new cell. The 'handoff' is said to be successful if there is at least one channel free in the new cell; otherwise, the call gets killed before it is completed. In the literature, the cellular systems have been widely studied. Guerin¹ shows by simulation that the channel occupancy time distribution is best approximated by an exponential distribution. Hong *et al.*² have developed an approximate analytical model and studied its performance characteristics. But in all the above studies simplifying assumptions are made on the motion of the mobiles. The system considered by us is more realistic than those dealt with in the literature. Further, in all previous studies, each cell is studied in isolation. This, as we show, is incorrect.

2.2. Model description

We consider a cellular communication system in which the new arrivals (not considering the calls handed off from other cells) at each cell form a renewal process. We assume that the mobiles move randomly with changes of velocity taking place at i. i. d. time intervals and the velocities form an i. i. d. sequence.

2.3. Analysis and results

The above communication system is modelled as an open network of queues. We have bounds for the time stationary distribution of number of customers at different nodes and we prove the existence of stationary distribution of the queue length vector for the entire system at both customer arrival epochs and at arbitrary instants of time. It has also been shown that the network is not of product form and thus we obtain bounds on the blocking probability. We develop network models which have product form solution and whose time stationary distributions stochastically upper bound the time stationary distributions of our system. To get bounds on the blocking probability we require bounds on the customer stationary distributions. Thus, we give some relations between time and customer stationary distributions. We also obtain insensitive upper bounds on the blocking probability at each cell site, in terms of the arrival rate of new calls, the mean of the channel holding time and the number of frequency channels at each cell. Since the mean of the channel holding time depends on the motion of the mobiles it is not readily known. We thus develop upper bound on the mean of the channel holding time in terms of the diameter of the cell and the mean of the velocity variable. We numerically compute the bound on the blocking probabilities for a small system and show that these bounds can be quite tight.

3. Satellite broadcast communication network

3.1. Introduction

We study a satellite broadcast communication network with a finite number of users and each of them having infinite buffers. An important factor to be considered in such networks is the large propagation delay. Due to this, access schemes such as CSMA and CSMA/CD, which perform well otherwise do badly in satellite communication environment. Polling, under light load, is also not efficient. Fixed channel assignment schemes such as TDMA perform well under heavy load (we show it in this thesis). Under light loads it can lead to large delays and inefficient use of the channel. On the other hand, the random access schemes like the ALOHA and its more efficient counterpart the slotted ALOHA are ideal when the network is lightly loaded. But as the load increases, the delays increase and the total throughput gets reduced. Thus what we would need is an adaptive system, which will adapt itself with the changing traffic pattern and also combine the advantages of random access mode when the system is lightly loaded with the advantages of fixed (or ordered) assignment mode when the load on the channel increases. Though there are a number of adaptive schemes proposed in the literature, most of them use reservation slots or

control subframes which would cause a lot of overhead under light loads. Also, because of the large propagation delay in satellite radio network, under light loads it can cause large delays.

3.2. Analysis and results

We show that under heavy load TDMA is better than many proposed algorithms in the literature. We also show that under very light load conditions, the slotted ALOHA is optimum. We use these two features to develop a protocol which will reduce to TDMA at heavy loads and to slotted ALOHA under light load conditions but will outperform them under intermediate loads. A similar scheme has been mentioned³ where they refer to an unpublished work of theirs. The difference between our work and theirs is that we prove stability of the system under more general conditions than theirs. They assume i. i. d. Bernoulli input process to each user. We also show the continuity of distributions and some stochastic comparison results for the queue length and the delay process. Further, we have developed a decentralised algorithm which will provide online the assignment scheme appropriate for the arrival rates to different users. These results have also not been obtained by Tsai and Chang³. The decentralised algorithm proposed does not need any extra information other than the feedback of the number of successes and collisions. Finally, we show some simulation results to show the utility of our multiple access scheme and also to show the convergence and overall performance of our dynamic scheme.

References

1. GUERIN, R. A. Channel occupancy time distribution in a cellular radio system, *IEEE Trans.*, 1987, VT-35, 89-99.
2. IJONG, D. AND RAPPAPORT, S. S. Traffic model and performance analysis for cellular mobile radio telephone system with prioritized and nonprioritized handoff procedures, *IEEE Trans.*, 1986, VT-35, 77-92.
3. TSAI, D. AND CHANG, J. F. A hybrid based contention TDMA technique for data transmission, *IEEE Trans.*, 1988, Com-36, 225-228.

Thesis Abstract (M. Sc. (Engng))

A study of hypercube-like networks using a multistage graph model by M. J. Shankar Raman

Research supervisors: Lawrence Jenkins and P. S. Nagendra Rao

Department: Electrical Engineering

1. Introduction

This thesis is concerned with the study of a class of communication networks that are used for interconnecting processing elements (PEs) and/or PEs and the main memory in multiprocessor systems. Such networks can be either static or dynamic. The results in this thesis pertain to a class of static networks called hypercube-like networks (HL-networks) proposed by Vaidya¹.

2. Multistage graph model

A multistage graph model (MGM) is developed for HL-networks which is shown to be similar to the well-known reduced graph model² (RGM) of self-routing permutation networks (SRPNs). An algorithm to derive the MGM for HL-networks and some of the properties of MGMs are discussed. It is also shown that for RGMs which satisfy the properties of the MGMs, an HL-network can be derived. A matrix model similar to the matrix model of SRPNs³ is developed and is used for deriving non-isomorphic HL-networks.

3. Routing

A correlation is established between the routing algorithms of SRPNs and HL-networks. It is shown that HL-networks have at least one and at most $n!$ destination tag-based (DTB) routing algorithms. An algorithm to ascer-

tain the feasibility of a given DTB-routing algorithm is presented. It is shown that whereas a baseline equivalent SRPN possesses bidelta property³, it may not be so with baseline nonequivalent SRPNs.

4. Fault tolerance

It is known that SRPNs can be made fault tolerant by providing an extra link and switching stages which guarantee more than one path between any source and destination. It is shown that extrastaging⁴ the MGM is equivalent to the addition of extra links in an HL-network. Using this, an algorithm to add extra links to HL-networks so as to enhance their fault tolerance is presented. Since all SRPNs are not extrastageable, a modified algorithm is presented which can be used to provide extra links in any HL-network to make it fault tolerant. It is established that if a particular set of links are made extra reliable in HL-networks, it is not necessary to add extra links.

5. Hyperstructures

It is also shown that these concepts could be extended to other class of networks which are named as hyperstructures. These could be considered as generalized HL-networks since these networks are obtained by considering radix- r ($r > 2$) number system instead of the binary number system used in HL-networks. The MGMs of hyperstructures are shown to be similar to the RGMs of SRPNs implemented through $(r \times r)$ ($r > 2$) switching elements. Routing algorithms are developed. An algorithm which systematically adds extra links to hyperstructures to enhance its fault tolerance is presented.

6. Conclusion

This thesis brings out the relationship that exists between static and dynamic interconnection networks. This is established using a graph model called the multistage graph model. It is shown that the theory behind routing, fault tolerance and matrix modeling of SRPNs could as well be applied to SINS. A new class of SINS called hyperstructures has also been proposed.

References

1. VAIDYA, A. S. *Hypercube-like networks*, Tech. Report, Department of Electrical Engineering, Indian Institute of Science, Bangalore 560 012.
2. AGARWAL, D. P. Graph theoretical analysis and design of multistage interconnection networks, *IEEE Trans.*, 1983, C-32, 637-648.
3. NAVANEETHAN, P. *BIPEDS: A new class of self-routing permutation networks for array processing systems*, Ph. D. Thesis, 1991, Department of Electrical Engineering, Indian Institute of Science, Bangalore 560 012.
4. RAVI SHANKAR, S. *Algorithms to test and implement fault tolerance in self-routing permutation networks*, Ph. D. Thesis, Indian Institute of Science, Bangalore, 1992.

A methodology to design performance driven multipliers using normal process complementary pass transistor logic (NPCPL) by Debabrata Ghosh
 Research supervisors: K. Parthasarathy and S. K. Nandy
 Department: Electrical Engineering

1. Introduction

A multiplier is an essential component in general systems as also in digital signal processing applications. Modern high-performance systems need on-chip multipliers with low latency and high throughput. Literature provides the designer with many a multiplier architecture ranging from small low-speed serial multipliers to large high-

performance parallel multipliers. The high-end multipliers fall into two broad classes—array and tree. Array multipliers, though very regular and compact, suffer in speed of operation. Tree multipliers, on the other hand, provide high speed, but are very irregular, consume a lot of silicon area and are hard to layout. Throughput of the multiplier, defined by the number of multiplications done per unit time, is also important, especially for DSP applications.

The problem with current architectures is that an architecture chosen for a given system's requirement cannot be used to meet a differing system's requirements. The architecture being fixed, multipliers with a limited range of latency, throughput and area can be generated. In this thesis, a generic architecture for multipliers is conceived. The goal of this thesis is to provide a methodology of designing a multiplier tailored to the requirements. It needs to be able to provide any value of area, latency and throughput (possible in a given technology) including the highest possible speed of operation. Desirable features of the target multiplier architecture are regularity, ease of layout and potential for automatic generation. The generic architecture proposed in this thesis attempts at incorporating all these features.

The performance of the multiplier, as much as of any other VLSI circuit, depends heavily upon the particular logic style used for implementing the architecture. Hence, new logic style called NPCPL (normal process complementary pass transistor logic) is developed to achieve low latency and high throughput simultaneously. This logic is 2–2.25 times faster than conventional CMOS and it allows pipelining to be introduced with minimal penalty of area and latency. NPCPL is used in achieving high performance in the generic multiplier architecture.

At the architectural domain, a new multiplier architecture called TWTXBB (tree of Wallace tree with XORs as building blocks) is proposed to cater to the high end of the user's requirement. This is faster than existing architectures, and hence, can be used for low latency applications. It is amenable to heavy pipelining rendering itself useful for applications requiring low latency and high throughput simultaneously.

2. NPCPL

High throughput and low latency designs are required in modern high-performance systems, especially for signal-processing applications. Existing logic families cannot provide both of them simultaneously. NPCPL can be used as a universal logic to provide finest grain pipelining without affecting overall latency or increasing the area. It does not require any special process steps and hence can be realised in a normal process technology as against the CPL proposed by Yano *et al.*¹ which uses threshold voltage adjustment of selected devices. The design procedure is described for (a) low latency, (b) high throughput, and (c) low area requirements. In addition to the various advantages, it is envisioned that NPCPL designs² can also be used to build ultra-high speed pipelined system without pipelining latches, *viz.*, wave pipelined³ digital systems, where the throughput achievable is beyond that permitted by the delay of a pipeline stage. A wave pipelined multiplier is designed in NPCPL and reported by Ghosh *et al.*⁴

3. TWTXBB: A low latency, high throughput multiplier architecture using a new $4 \rightarrow 2$ compressor in NPCPL

TWTXBB is intended for high performance characterised by both low latency and high throughput. Existing fast multiplier architectures, like Wallace tree architecture⁵, result in an irregular layout with a complex interconnection pattern. TWTXBB outperforms Wallace tree in speed of operation by 33%. It is highly regular rendering itself amenable to automatic generation. The multiplier achieves its high speed from both a new architecture and the logic-style NPCPL. To the best of our knowledge this is the only architecture which provides lowest latency (for a given process technology) and potential for automatic generation at the same time. Yet another attractive feature of this architecture is that it can provide both low latency and high throughput simultaneously. An elegant pipelining scheme can be tailored to this architecture to achieve fine grain pipelining with insignificant overhead of latency and area.

4. Architectural synthesis of performance-driven multipliers with accumulator interleaving

As already mentioned, VLSI multipliers assume different characteristics in terms of latency, throughput and area for different target applications. There is no integrated design approach to cater to these widely varying user re-

quirements. We propose a methodology of automatically generating a multiplier from the user's specifications of latency, throughput, and area⁶. The entire gamut of multipliers, starting from low area, moderate performance multipliers to high performance ones with low latency and/or very high throughput is captured in this procedure. The architecture comprises a smaller core, a front-end server (FES) and a back-end processor (BEP) which allows to use the basic core repetitively for multiplication of larger numbers. Through a novel method of accumulator interleaving the multipliers designed using the proposed methodology support better performance compared to conventional approaches. Thus the proposed methodology can be used for synthesis of multipliers occupying any place (feasible in a given technology) in the A-L-T (area, latency, throughput) space, subject to an affordable power dissipation.

5. Conclusion

In this thesis, an integrated design methodology to generate performance-driven multipliers is discussed. The multipliers achieve their high performance form the NPCPL logic. The TWTXBB architecture is used for multipliers requiring very low latency or low latency and high throughput simultaneously.

There is scope for doing further research in decreasing the static power dissipation and improving noise margin of NPCPL without sacrificing performance. The TWTXBB architecture may also be tested with some other logic.

References

1. YANO, K. *et al.* A 3.8 ns 16×16 -b multiplier using complementary pass-transistor logic, *IEEE J.*, 1990, SC-25, 388-395.
2. GHOSH, D. *et al.* NPCPL: Normal process complementary pass transistor logic for low latency, high throughput applications, *VLSI Design*, '93-The Sixth Int. Conf. on VLSI Design.
3. DEREK WONG *et al.* Designing high-performance digital circuits using wave pipelining: Algorithms and practical experiences, *IEEE Trans.*, 1993, CAD-12, 25-46.
4. GHOSH, D. *et al.* A 400 MHz wave-pipelined 8×8 -bit multiplier in CMOS technology, *Int. Conf. on Computer Design (ICCD)*, 1993.
5. WALLACE, C. S. A suggestion for a fast multiplier, *IEEE Trans.*, 1964, EC-13, 14-17.
6. GHOSH, D. *et al.* Architectural synthesis of performance-driven multipliers with accumulator interleaving, *30th Design Automation Conf.*, 1993.

Thesis Abstract (M. Sc. (Engng))

Evanescent coupling between fiber and planar waveguides by R. Mahendra Prabhu

Research supervisor : A. Selvarajan

Department : Electrical Communication Engineering

1. Introduction

Photonics has emerged as an important area over the past three decades. Optical waveguides like fiber have been made with minimum losses. Also the technology has developed rapidly in fabricating various other kinds of optical waveguides like planar, channel waveguides, etc. Coupling of light into waveguides is necessary for characterizing and practical applications of optimal waveguides. The evanescent coupling between fiber and planar waveguide is analysed using finite beam propagation method (FDBPM) with nonuniform mesh configuration.

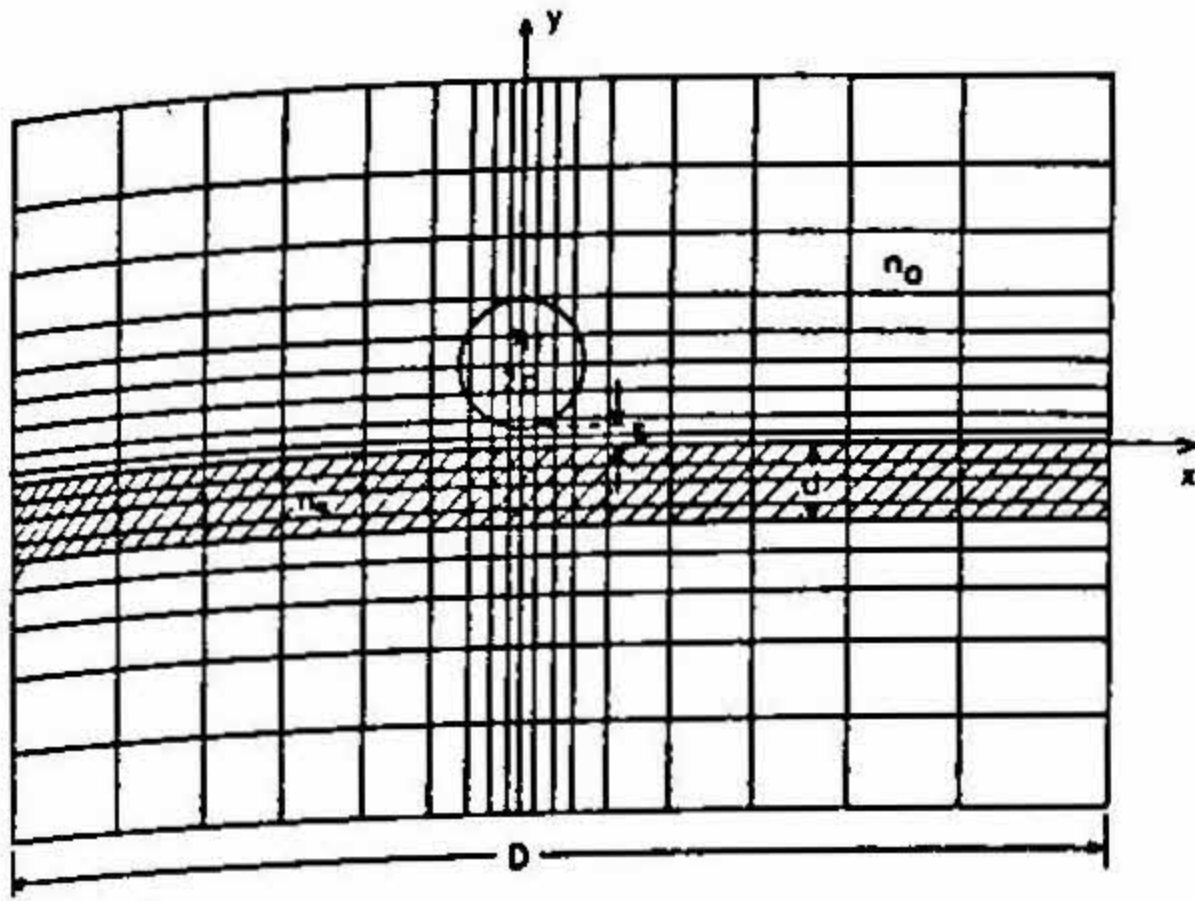


FIG. 1. Cross-section view of the fiber and slab waveguide inside the computation window.

Also the fiber and waveguide are made tapered to increase the coupling between them. This aspect is also studied in detail using FDBPM with small modification.

2. Analysis

Though there are various other types of beam propagation methods like fast Fourier transform BPM, FDBPM¹ was chosen because it is numerically stable for strongly guided cases and for large propagation distances. Non-equidistant grid spacing can be applied in FDBPM which provides a large area of study. In FDBPM one applies the finite difference operator to the parabolic or Fresnel wave equation. On knowing the field at any z , one can find the field at any arbitrary distance $z + \Delta z$, and thus one can iteratively find the field that propagates through the considered structure.

Optical system consisting of an unclad fiber core suspended at a constant distance parallel to the surface of a planar waveguide is used in this study as shown in Fig. 1. Here the evanescent tail of the fiber is coupled into the waveguide as the wave propagates and is used to transfer the power from fiber to waveguide. Study is done for a particular refractive index of the fiber and different indices of the slab waveguide. When the refractive index of

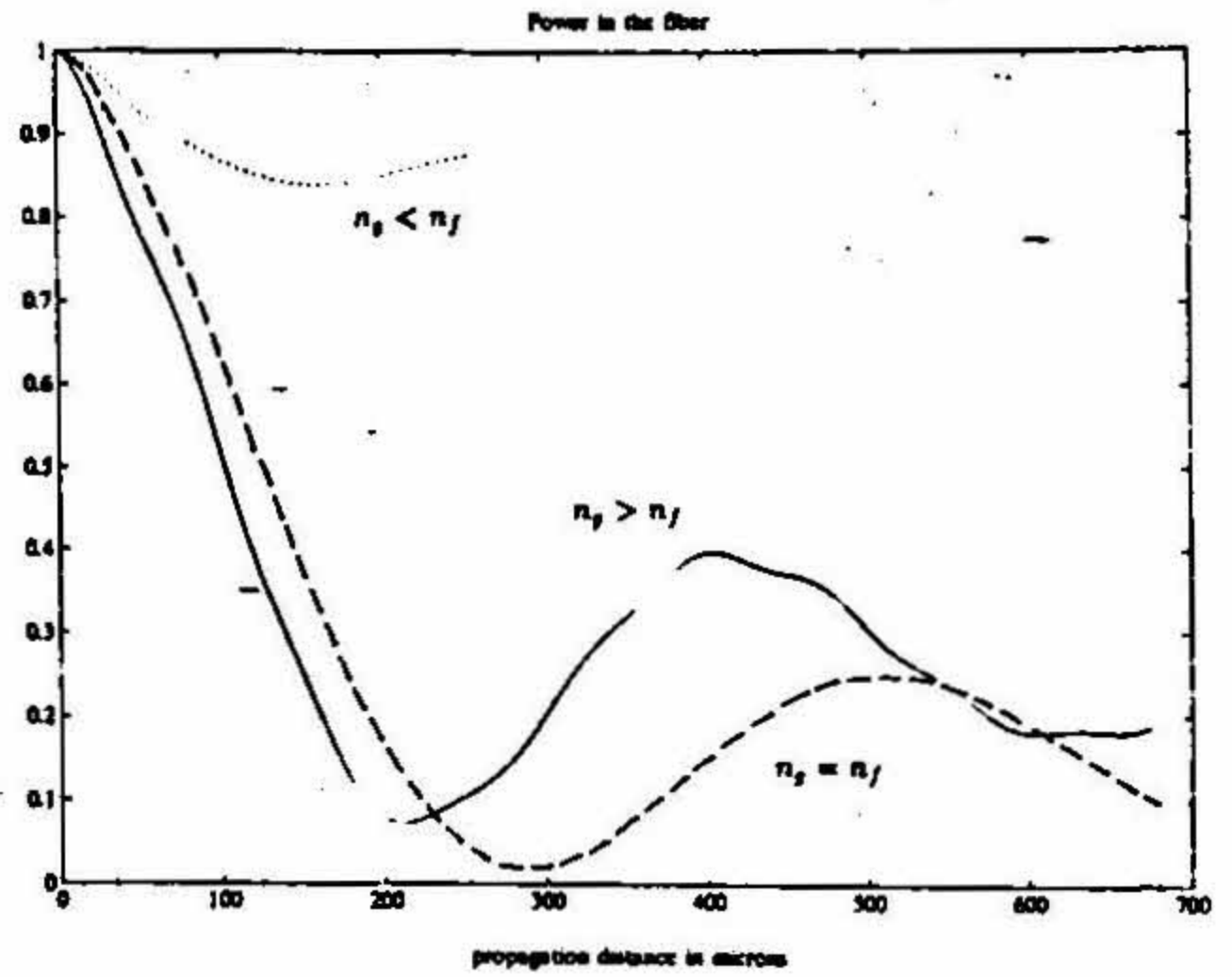


FIG. 2. Power remaining in the fiber as function of propagation distance for three step-index slab cases.

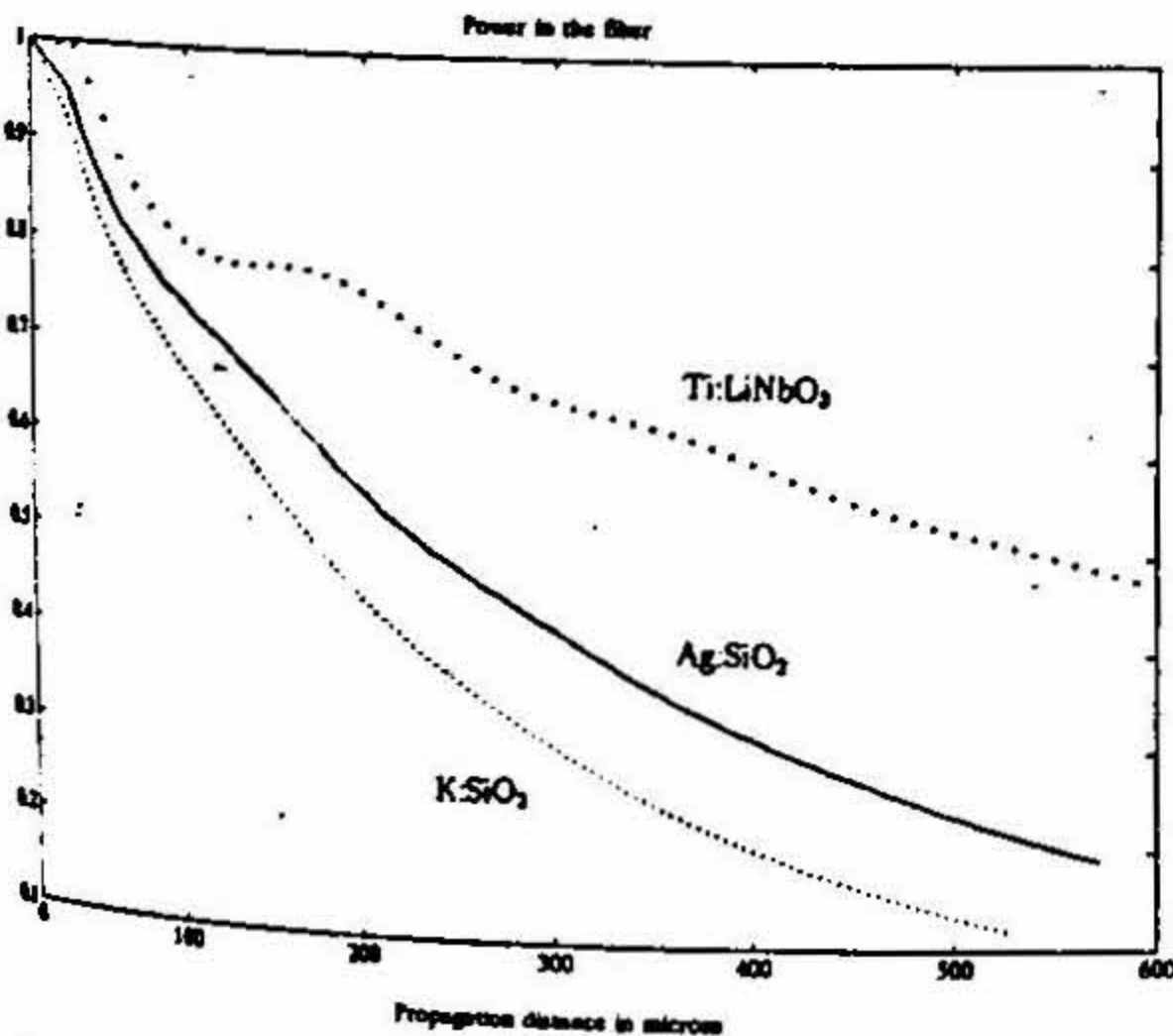


FIG. 3. Power remaining in the fiber as function of propagation distance for three graded-index slab cases.

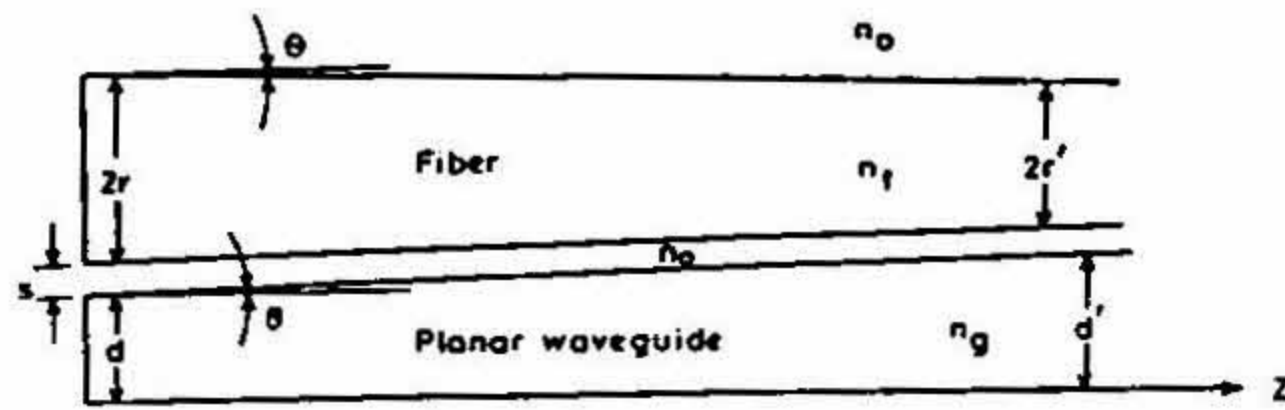


FIG. 4. Tapered fiber and planar waveguide.

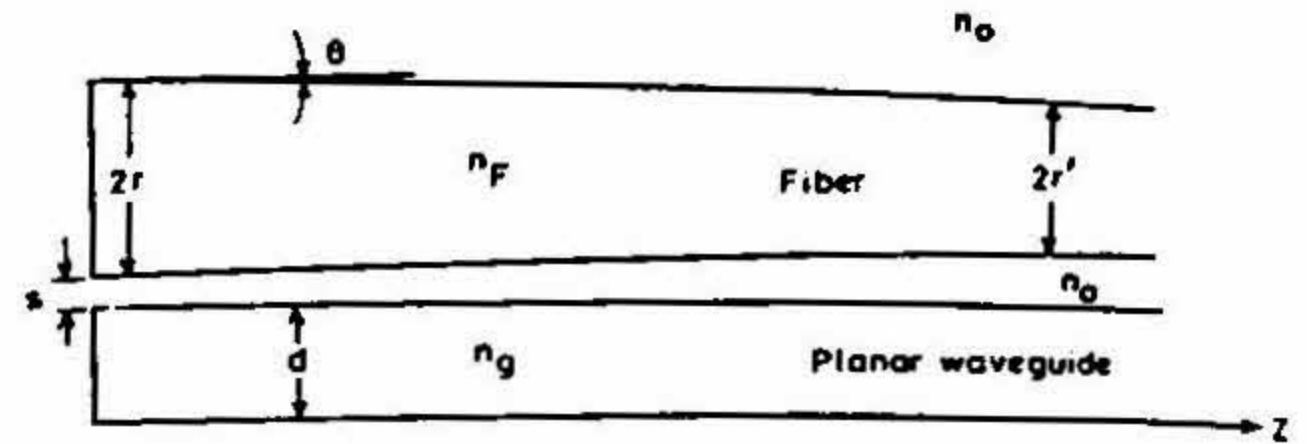
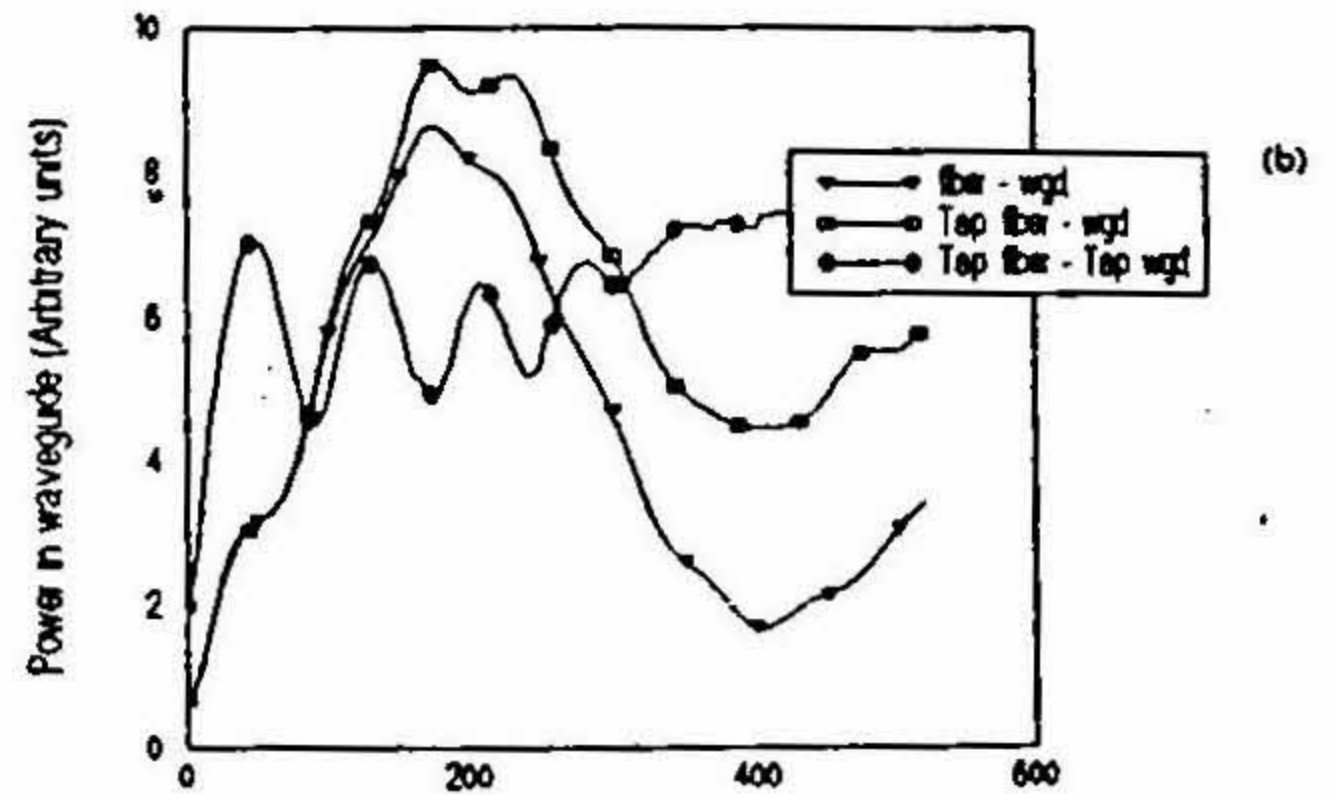
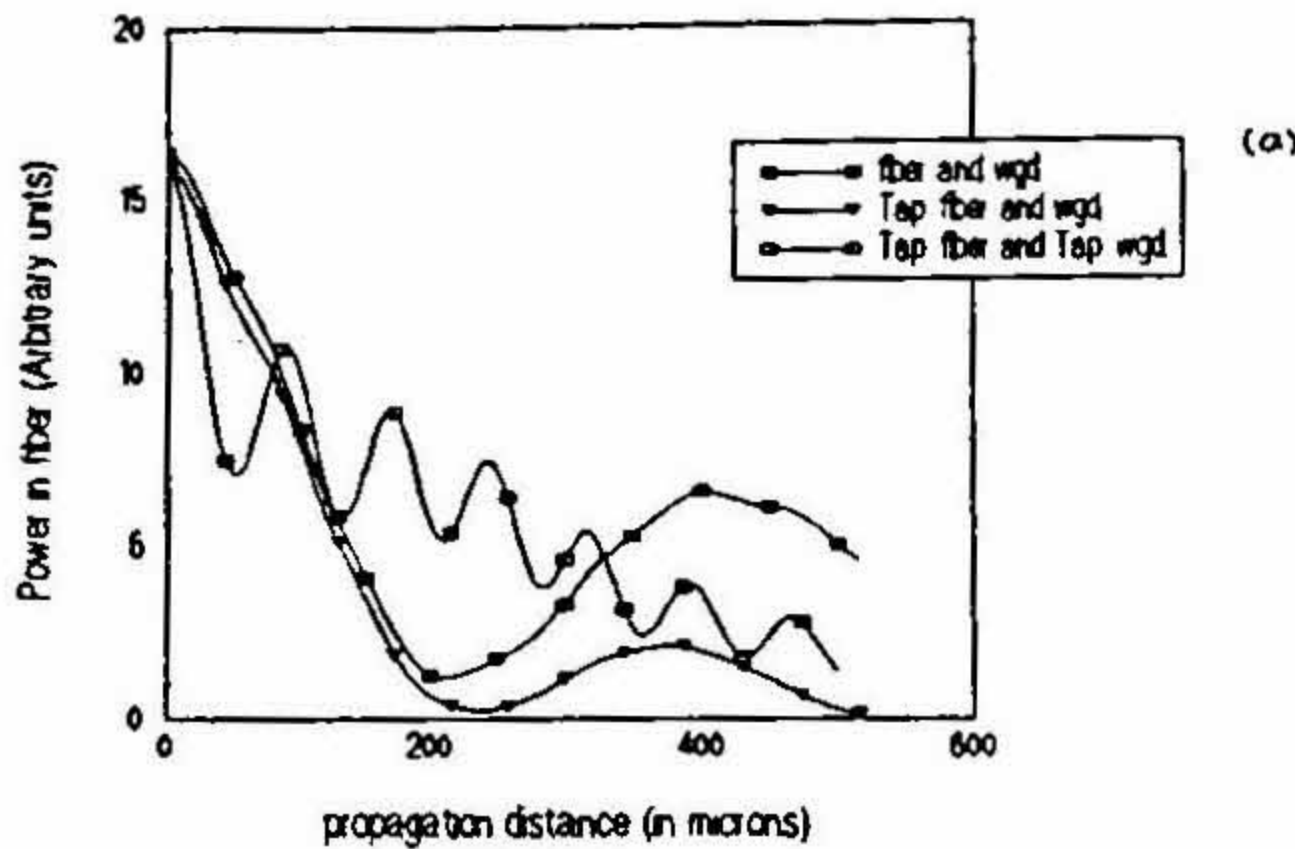


FIG. 5. Tapered fiber and tapered planar waveguide.

FIG. 6. Power in fiber and waveguide—comparative plot ($n_g > n_f$). a. Fiber power vs propagation distance, b. Waveguide power vs propagation distance.

the fiber is greater than that of the waveguide, no power transfer takes place from fiber to the waveguide; when the refractive index of the fiber and the waveguide are the same, the power oscillates back and forth; and when the refractive index of the waveguide is larger than that of the fiber the power in the fiber falls drastically and at the same time many lateral modes in the waveguide are excited. Figure 2 shows the power in the fiber for the above considered cases. These are in agreement with the results obtained by coupled mode theory by Marcuse². Coupling between step-index fiber and graded index slab waveguide is also studied. Titanium diffused lithium niobate waveguide, silver and potassium ion exchanged waveguides are considered in this study (Fig. 3). The index profile in the waveguide is assumed to be of error function complement type.

The role of junctions between large-core multimode optical waveguides and small-core guides in integrated optical devices has led to an interest in tapering between fiber waveguides³. Study is done on coupling between tapered fiber-slab waveguide and tapered fiber-tapered slab waveguide (Figs 4 and 5). The FDBPM is modified for tapered waveguide application⁴. Coupling between tapered fiber-slab waveguide is studied for various taper angles (0.11° , 0.25° , 0.5° and 1°) and as the taper angle decreases, there is good coupling between them. The power in fiber and waveguide when the refractive index of the waveguide is greater than the fiber, for all the cases, is shown in Fig. 6.

3. Conclusions

The power remaining in the fiber as a function propagation distance for various cases is studied. The coupling from fiber to glass waveguides is found to be better compared to the case of fiber to lithium niobate waveguides. When the slab waveguide is also tapered along with the fiber so that they are at a constant distance apart, the coupling from fiber to waveguide is better compared to all the other cases.

References

1. CHUNG, Y. AND DAGALI, N.

Analysis of z-invariant and z-variant semiconductor rib waveguides by explicit finite difference beam propagation method with non-uniform mesh configuration, *IEEE J.*, 1991, QE-10, 2296–2305.

2. MARCUSE, D. Investigation of coupling between a fiber and an infinite slab, *IEEE J. Lightwave Technol.*, 1989, 7, 122-130.
3. NELSON, A. R. Coupling optical waveguides by tapers, *Appl. Opt.*, 1975, 14, 3012-3015.
4. HERMANSSON, B., YEVICK, D. AND DANIELSEN, P. Propagating beam propagation analysis of multimode waveguide tapers, *IEEE J.*, 1983, QE-19, 1246-1251.

Thesis Abstract (M. Sc. (Engng))

A method of fault diagnosis in a wave soldering system by Sreenath Settur

Research supervisors: M. Satyam and M. H. Kori (CDOT)

Department: Electrical Communication Engineering

1. Introduction

In an electronic manufacturing system, the card assembly is a critical stage. In this, the components are mounted and firmly connected on to the board fulfilling the basic functional requirement besides giving necessary mechanical strength and electrical connectivity on long-term basis.

Of the various interconnecting techniques, soldering is the most versatile one. The hand soldering with the soldering iron and mass soldering with the wave soldering machine are important methods under this.

Wave soldering is the most popular mass-soldering technique and more than 85% of the PCBs soldered throughout the world are wave-soldered. In this technique, the PCB mounted with the components moves on a conveyer, the solder side of the PCB and the component leads get fluxed, preheated and then get in touch with the wave of solder for a fixed time (typically 1-5 s), before moving out of the conveyer.

The quality of the soldering process determines the quality and reliability of the assembled PCB and thus, in turn, limits the quality and reliability of the electronic equipment. Each of the process stages contributes to certain deficiencies and they manifest as defects in an assembled card. A few investigators [1 thru 10] have attempted to explain the defects and causes and possible remedies for the same. However, there are certain limitations in these, viz., the defects are considered individually and the solutions suggested are subjective.

In this study, an attempt has been made to arrive at a methodology to obtain the order of causes responsible for the defects, based on the information on probability of a particular cause giving rise to a defect.

2. Proposed fault diagnosis method

To begin with, a detailed study was made to understand the overall card assembly process and this was carried out on the wave solder system, model TDL (Hollis make), USA, which uses water-soluble flux. This machine has a motorized conveyer, foam fluxer, preheater, solder bath and control unit.

The various defects that have been observed on the cards soldered using the above machine have been identified to be of 19 types, which are as follows: Insufficient hole filling, dewetting or nonwetting, solder voids or outgassing, excess solder, icicles, bridging, webbing, solder balls or splatter, rough or disturbed solder, grainy solder, cold solder, discolored solder, components lifted, flux entrapped, masking failure, blistering, measling, and warpage.

Each defect was understood clearly with respect to their causes. After carefully analyzing the defects and causes it was noted that there are two categories of reasons, viz., machine- and non-machine-controllable reasons.

Machine-controllable causes are identified to be the process settings that can be adjusted such as solder temperature (high/low), solder wave height (high, low or uneven), preheat temperature (high/low), conveyer speed (high, low), conveyer vibration, conveyer angle (high/low), fluxer problem, solder contamination, specific gravity of flux low or flux contamination, board removed early, return board, bad fixture, excessive/poor oil intermix.

It was further observed that a defect is manifested because of the influence of one or more causes. Similarly, a cause may be responsible for one or more defects simultaneously. However, the degree of influence varies. This called for a study of what 'causes' contribute to what 'extent' in the manifestation of a given defect.

In the case of machine-controllable causes, it was attempted to study the degree of influence each cause has for a given defect independently. A large number of production cards were observed very carefully to get an estimate of the degree of influence. For example, if a cause x contributes 80% of the times to a defect y , the degree of influence is defined to be 0.8. Four levels were defined, *viz.*, 1.0, 0.8, 0.5, 0.0 depending on the level of influence of that cause in influencing the defect in question. In cases where such a number is in between these, it is taken as the next higher number. These numbers are called the 'weightage factors'. For each defect such weightage factors are estimated.

In the case of single defect, the weightage factors directly give the order of causes according to their level of influence. However, when more than one defect is present, it is necessary to adopt a criteria to look for the cause that affects most, and the next cause which is less probable and so on till the least. This technique was followed to identify the important causes and to rectify them; later the observations were continued to check the accuracy of the remedy suggested.

The reasons which are outside the machine-controllable factors were identified to be design, fabrication and assembly related and these are as follows: PCB design-related causes—Large plane on component side/solder side, hole to lead ratio too small/too large, large holes, orientation of components and tracks, improper weight distribution on the PCB, track width and track spacing; fabrication-related causes—contaminated or oxidized PCB, mask misregistration, moisture-exposed laminate, defective mask material, misregistration of holes or pads, warpage of PCB, rough PTH and exposure of epoxy glass; assembly-related causes—contaminated PCB/component leads, component leads too long/too short, excessive/insufficient mask, and bad handling of PCB.

In these cases, suggestions are to be fed back to the designer, vendor or assembly, respectively, for suitable preventive measures to be taken. These are also analyzed in a similar way as those of machine-controllable.

It may also be noted that the complexity of analyzing the defects increases because of the fact that defects do not occur in isolation, but occur together and the causes are also not independent. They are by and large collective (a few interacting positively and a few interacting counter-positively). Hence it was felt that a simple algorithm which carries out this analysis based on the information on the defects and provides probable causes responsible for the defects, is needed.

An algorithm was developed with a view to arrive at a suitable software package (DOWS) that helps in the diagnosis of the defects that may arise in the assembly line and to prompt the probable solutions when soldering defects observed are fed in from the set of defects. The preassigned weightage factors are taken for each of the defects and they are added correspondingly and arranged in the descending order of the cumulative weightage factors. The final prompting that appears at the end would be in the form of suggestions in each case.

The DOWS package is developed in C language and is interactive and is user-friendly.

3. Performance evaluation of DOWS package

The DOWS package is verified in a careful manner as follows: The settings of the machine were deliberately changed and the defects observed. These observations are made on three cards in each of the settings. The settings modified are solder and preheater temperatures and conveyer speed. The defects, thus observed, were fed into the DOWS package and the solutions/suggestions for the process are noted. This indicated that the top two (or three) suggestions match with the setting modifications carried out, and in cases of single setting modification, it appears within the top two suggestions. It may be noted that all the suggestions are not the real causes. However, it would be necessary to monitor them also for ascertaining that they are not the causes and to ensure that the suggestions being implemented give requisite improvement.

The effectiveness of the DOWS package is also tested in the actual production line (June–November 1992) and found to predict the causes satisfactorily.

4. Conclusions

After a comprehensive study made in the actual manufacturing line—card assembly using a wave soldering machine—though 19 types of defects and various causes that contribute to these are identified, it was noticed that only a few defects and a few causes are common. These may be termed dominant defects and dominant causes.

The dominant defects include fundamental soldering defects such as poor wetting (*i.e.*, non-wetting and de-wetting) and others like bridges, icicles and appearance-related defects. The dominant causes include machine settings (*e.g.*, solder bath and preheater temperatures and conveyer speed, etc.), and others like solderability and the material quality (of solder and the flux).

The package developed has the following limitations:

1. It presents all the probable causes, from which the top one or two or three causes only may be the actual ones and the exact cause has to be ascertained before modifying the settings. Further, the remedies suggested are qualitative, and exact variation to be introduced is not indicated.
2. The results as presented in this thesis are based on the data available from a particular type of machine, and are expected to be applicable in general. However, the user is advised to check whether the weightage factors are suitable for his set-up.

References

1. THWAITES, C. J. *Soft soldering handbook*, ITRI Publication no. 533, 1977.
2. MANKO, H. H. *Solders and soldering*, 1964, McGraw-Hill.
3. WASSINK, R. J. K. *Soldering in electronics*, 1984, Electro-Chemical Publications Ltd, UK.
4. GIOVANNI LEONIDA *Handbook of printed circuit design—manufacture, components and assembly*, 1981, Electro-Chemical Publications Ltd, UK.
5. LAMBERTT, L. P. *Soldering for electronic assembly*, 1988, Marcel Dekker.
6. WOODGATE, R. W. *The handbook of machine soldering*, 2nd edn, 1988, Wiley.
7. KEELER, R. Defects in wave soldered through hole connections, *Electronic packaging and production*, July 1990.
8. Troubleshooting soldering problems, *Electronic production*, December 1989, Electrovert, UK.
9. *Troubleshooting checklist for the wave soldering of PWBs*, IPC-TR-460 A, The Soldering Subcommittee, IPC Technical report, Nov. 1973 revision A, February 1984.
10. *TDL—Instruction manual*, Hollis.

Thesis Abstract (M. Sc. (Engng))

Guided wave acousto-optic interactions in LiNbO_3 by P. Annachelvi

Research supervisor: A. Selvarajan

Department: Electrical Communication Engineering

1. Introduction

The rapid development in the area of optical communication has greatly influenced the field of integrated optics which involves a number of techniques and technologies brought together to support a wide variety of

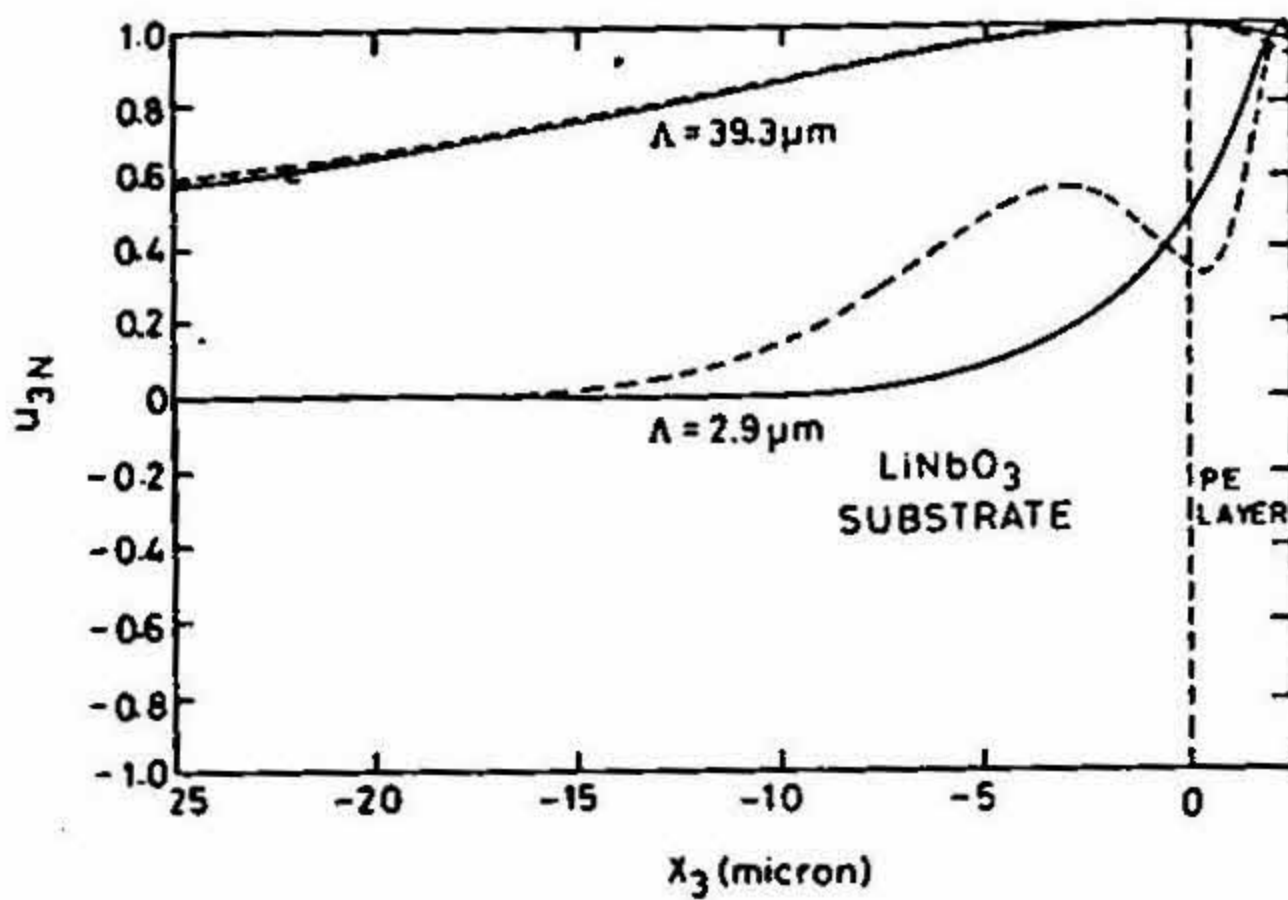


FIG. 1. Normalized mechanical displacement u_{3N} in PE: LiNbO₃ through the present analysis (dashed curve) and in bulk LiNbO₃ using von Helmholtz's analysis (solid curve); waveguide depth = 2.5 μm .

functions such as switching, filtering, interferometry, signal processing, sensing, etc. The acousto-optic (AO) technique making use of the surface acoustic waves (SAW) and the guided light is very promising and has given rise to considerable activity for a period of several years. Many AO experiments have been performed and devices realized, using different materials and waveguide structures. Yet, there has not been many reports on the rigorous computation of basic AO interaction in specific materials and waveguiding structures. This thesis deals with a theoretical analysis of AO interaction in the specific case of LiNbO₃ waveguides by rigorously computing the strain distributions and the optical mode fields.

2. Analysis

In the present analysis, practical waveguides such as (i) proton-exchanged (PE) and (ii) titanium-indiffused proton-exchanged (TIPE) waveguides in LiNbO₃ are considered. The well-known solution for the optical mode field distribution for the case of step-index asymmetric planar waveguides is used for the step-index proton-exchanged waveguides. The exact solution is obtained for the case of layered waveguide with both step and graded profiles present in the two layers of the waveguide. The exponential profile is assumed for the graded index region. Such a configuration of layered waveguide exists in TIPE waveguides. By matching the field solutions corresponding to the exponentially profiled graded index region and that corresponding to the step-index region at the interface between the two layers, the characteristic equation to determine the propagation constant is obtained. The mode distribution of the combined structure is given by the field solutions in the individual waveguiding layers which are matched at the boundary.

The theory leading to the solution of SAW distribution in bulk medium and layered medium is applied to the case of bulk LiNbO₃ and proton-exchanged LiNbO₃, respectively. The former case is similar to the earlier analysis by von Helmholtz¹. For the latter case of proton-exchanged waveguides, the following assumptions are made: The proton-exchanged region forms a homogeneous, nonpiezoelectric layer on the piezoelectric LiNbO₃ substrate. The crystalline structure of the PE medium is trigonal. The values of the material constants C_{ijkl} , C_{ijk} , ϵ_{ij} , ρ , and the dispersion curve (ν vs kh) taken are valid for PE waveguides fabricated in dilute melts containing 0.25 to 2.00 mol% of lithium benzoate². The relevant material constants corresponding to the PE layer and LiNbO₃ substrate are used in the calculation and YZ-cut configuration is chosen. In finding out the partial field amplitudes, the 12×12 boundary condition matrix reduces to 8×8 . The partial field amplitudes are normalized to the SAW power flow $P_{\text{SAW}} = 1$ W/m and $\omega = 1$ rad/s. The resulting distributions of u_1 , u_3 and ϕ corresponding to the SAW are found to be greatly modified in the presence of the PE layer, when the layer dimension is comparable to the acoustic wavelength Λ . When Λ is much greater than the waveguide depth, then the distributions resemble that in the bulk LiNbO₃. The normalized distribution u_{3N} is given in Fig. 1.

The AO interaction efficiency is a sensitive function of the spatial distributions of the optical and the acoustic distributions through overlap integral Γ . Γ depends on the waveguide parameters and the frequency of SAW. The determination of Γ and its frequency response is carried out for different cases by considering SAW (i) bulk LiNbO₃, (ii) PE layer in LiNbO₃. Figure 2 compares the results of the two cases.

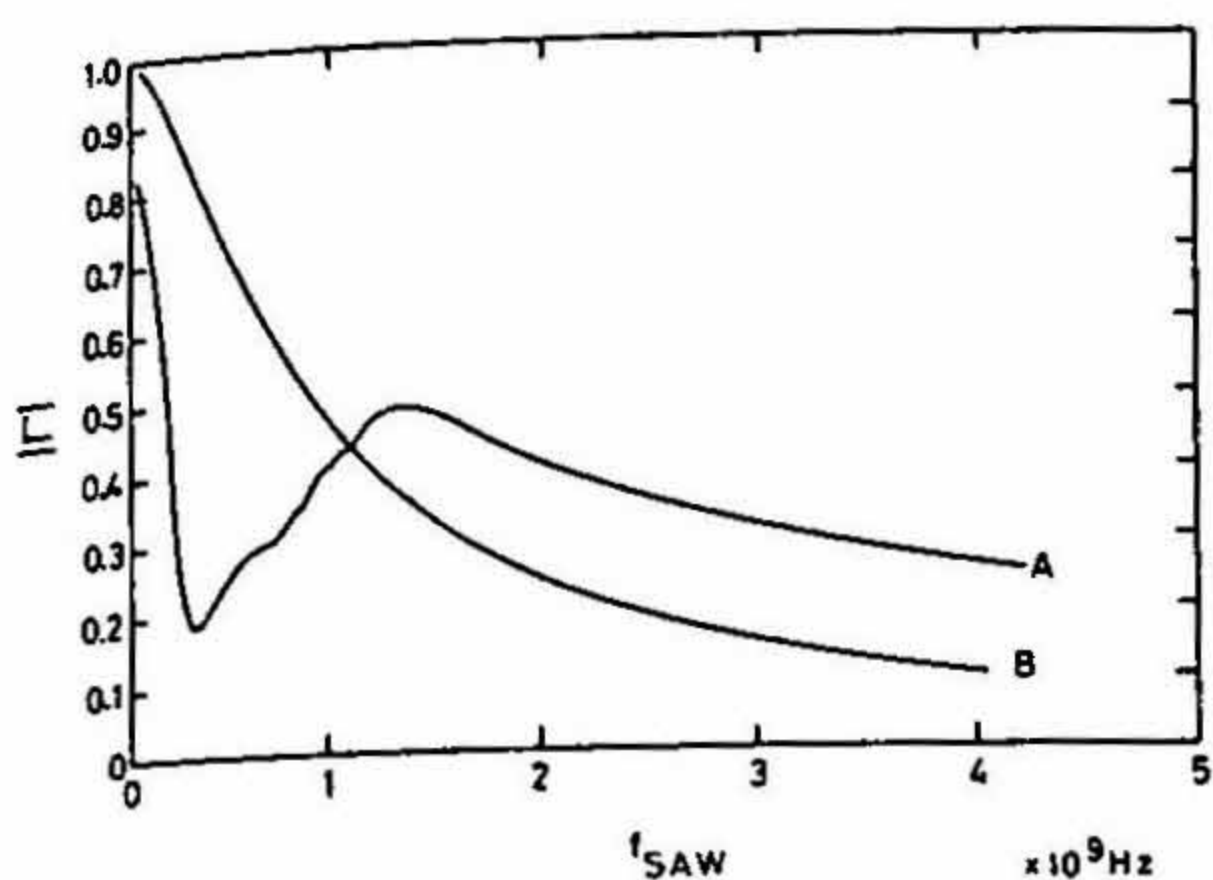


FIG. 2. Frequency response of the overlap integral in the present case (A) and in vol Helholt's case (B).

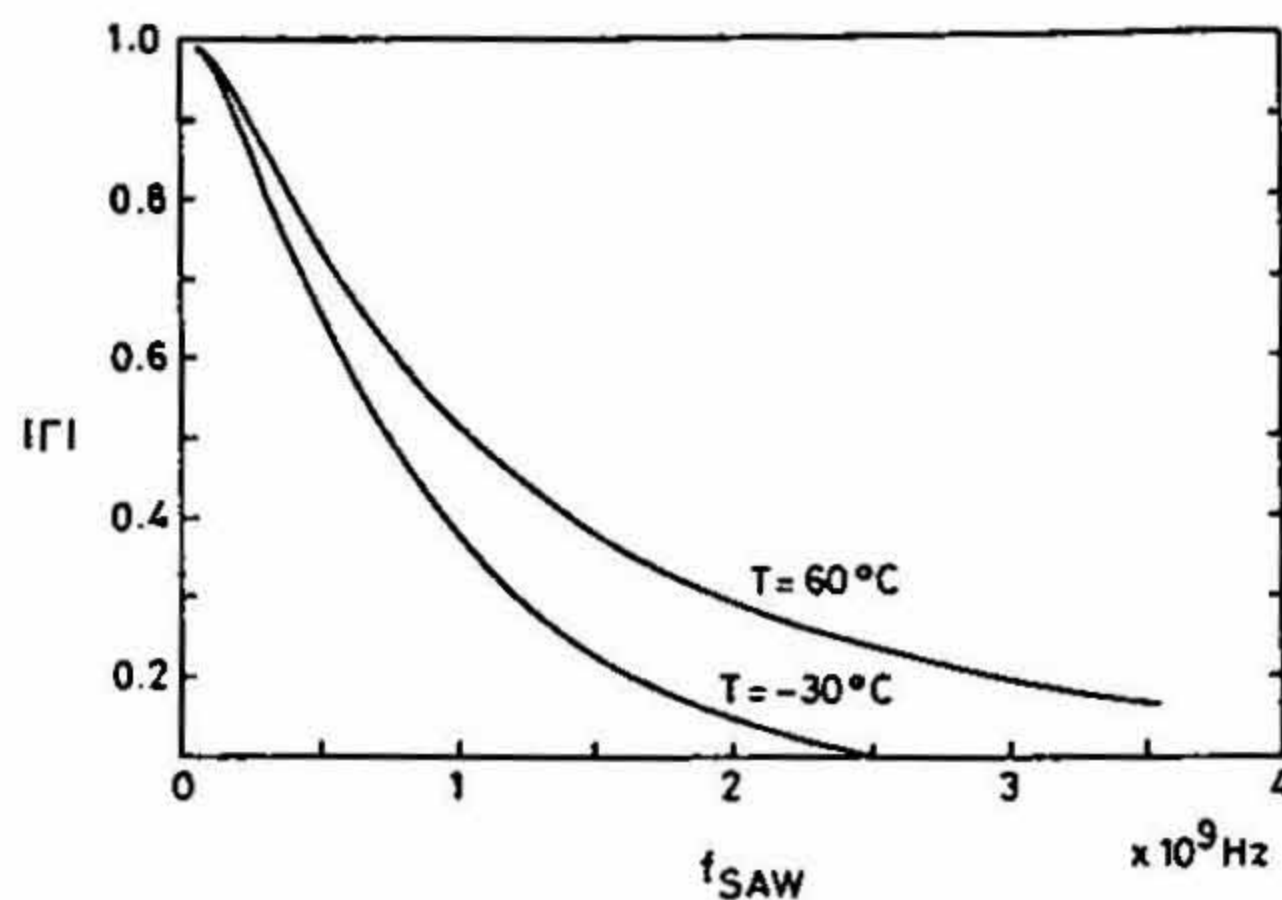


FIG. 3. Temperature dependence of the overlap integral at different frequencies.

3. Results and conclusions

The step-index proton-exchange waveguides are found to have better overlap and hence more AO efficiency than the diffused waveguides. The temperature dependence of the material constants shows that the influence of temperature on the overlap is significant only at high frequencies (Fig. 3). The present improved analysis shows that the frequency response of the AO interaction changes depending on the waveguide thickness relative to the acoustic wavelength.

References

1. VON HELMOLT, C. H. AND SCHAFFER, C. Efficiency of guided wave acousto-optic interactions for selected cuts in LiNbO_3 , *J. Opt. Commun.*, 1987, 8, 49-56.
2. BIEBL, E. M. AND RUSSEK, P. Elastic properties of proton exchanged LiNbO_3 , *IEEE Trans. Ultrasonics Ferroelectrics Frequency. Control*, 1992, 39, 330-334.

Thesis Abstract (M. Sc. (Engng))

Performance-reliability modeling of a distributed fault-tolerant flight computer system by P. V. Kamesh

Research supervisors: N. Viswanadham and S. K. Chaudhury

Department: Computer Science and Automation

1. Introduction

The design goals of modern advanced military aircraft include high maneuverability, light weight and fuel efficiency which forces the designers to develop a structure for the aircraft which is highly unstable. This calls for a fine degree of control surface actuation to maintain stability of the aircraft during flight which in turn necessitates the use of highly reliable computers in the control of the aircraft. Rapid advances in VLSI technology has resulted in the development of advanced integrated digital avionic systems configured not to lose the key functions such as aircraft stability augmentation even in the presence of failures. Fault-tolerant distributed computer systems are thus increasingly being employed for this kind of mission critical aerospace applications^{1,2}.

The designers of these computer systems are thus faced with the problem of finding an architecture which can meet all performance and reliability requirements. Several computer-aided system evaluation tools are available for performance evaluation of these computer systems given a faithful model. But the process of modelling itself still remains an art and depends to a large extent on the physics of the particular system being modeled and the skills and knowledge of the designer. In this thesis, we illustrate the modelling and evaluation of the performance

and reliability of a representative state-of-the art computer system aboard a military aircraft using stochastic reward nets (SRN)¹ models and object-oriented discrete event simulation.

2. Architecture of the proposed flight computer

The computer system consists of several processor nodes which are interconnected through three dual redundant MIL-STD-1553B serial bus interfaces. One of the processor nodes of the system is nominated as a master computer which is responsible for the functions of supervision, redundancy management, system wide health monitoring and also for reconfiguration control. The detection of faults and reconfiguration of the system is carried out by the master. The communication protocol is strict master-slave with broadcast features. The master is connected to all the three buses, while the nodes are connected to one or more buses depending upon the reliability requirements of the node. The real-time workload of each node consists of a set of periodic tasks which vary with the phase of operation of the aircraft such as take-off, level flight, landing, etc. The processor node also processes aperiodic tasks having higher priority.

3. Performance-reliability models for the flight computer

We perform a preliminary performance analysis of a single processor node with a single periodic task and the presence of aperiodic tasks. Then we develop detailed performance models for a node of the computer system using SRNs. These models take into account the priority of the real-time tasks, real-time scheduler actions and deadline failures. We determine various performance measures such as processor utilization, throughput, deadline failure probability and number of jobs lost, etc., in various phases of operation and under different failure conditions.

We then construct two-level hierarchical model consisting of

- (1) A phase-failure SRN model which captures varying phase conditions and the failure behaviour of the processors and the buses within the node.
- (2) A fault handling model which captures the different faults that can occur in the node and the system's response to these faults. The detection/reconfiguration process is also represented in this model.

The above models are then combined by an approximation using a two-level hierarchical model. The approximation is based on the fact that the rates in the fault-handling model are order of magnitude faster than those in the phase-failure model. The measures obtained in the performance model are then assigned as reward rates in the phase-failure model to obtain composite performability⁴ measures. Besides this we compute the deadline failure probability over a mission period by combining the phase-failure model and the deadline failure probabilities in each phase. We vary various parameters of the model such as the detection probabilities, failures rates, transient fault rates, etc., to see their effects on the performability of the system.

We formulate a performance simulation model of the distributed system in terms of an object-oriented paradigm. In this model we have overcome some of the limitations faced during analytical modeling. For example, we have modeled the scheduler action more precisely by being able to dispatch periodic tasks at regular intervals. We were constrained to use a five-stage Erlang distribution in the SRN models. Besides these, we are able to model some of the finer details of the system operation such as the MC's transactions, etc. We follow the object-oriented design approach in developing the model. In this process we show the compatibility of the object-oriented paradigm with the representation used in simulation. An implementation of the above is carried out in the object-oriented language C ++ . It is made clear how the above implementation focuses on the description of the problem rather than the algorithms for solving the problem, strengthening our support for the use of the object-oriented approach. A number of simulation runs are carried out to obtain various performance measures within certain confidence intervals. The simulation results match the analytical results within an error of 5%.

4. Contribution of the thesis

The contribution of this thesis has been the formulation of hierarchical performance-reliability (performability) models of a fault-tolerant real-time system taking into account the following factors: scheduling algorithm, deadline failures, phase of operation, processor failures, bus interface failures and imperfect coverage/fault handling.

The second contribution is to use the above models to obtain composite performance–reliability measures such as deadline failure probabilities, processor utilization, node failure distributions, etc. The results obtained from the analysis of the above models are of immense practical importance during the design phases of the flight computer system as they help identify the deficiencies of the design in meeting the performance–reliability requirements.

Using the above models, we computed the processor utilization for various job classes and mission scenarios. In order to determine minor frame frequencies meeting the utilization criterion and the deadline failure constraint, we computed processor utilization and deadline failure probability for various minor frame frequencies. It turns out that for the given processing power and the existing minor frame frequency, the deadline failure probability in the worst case is $4.2323e-3$ which does not meet the reliability requirements. We have determined that unless the processing power is increased four fold, the processor node cannot meet the reliability requirement with the existing minor frame frequency.

We also evaluated the effect of various reliability related parameters such as failure rate, detection probability, etc., on the deadline failure probability quantifying the effect of reliability on performance. In this case, we found that only the failure rate had a significant effect on the deadline failure probability.

Finally, we computed the node failure distribution and its sensitivity to various reliability factors. Once again, we found that the failure rate had the maximum effect on the failure distribution. The next most sensitive factor was the transient rate followed by the detection probability. The reconfiguration probability was found to have negligible effect.

References

1. HOPKINS, A. L., SMITH, T. B. AND LALA, J. H. Ftmp—a highly reliable fault tolerant multiprocessor for aircraft, *Proc. IEEE*, 1978, 66, 1221–1239.
2. LALA, J. H. *et al.* Advanced information processing system (aips) based fault tolerant architecture for launch vehicles, *In Proc. IX AIAA/IEEE Digital Avionics Systems Conf*, pp. 125–132, 1990.
3. CIARDO, G., MUPPALA, J. AND TRIVEDI, K. S. On the solution of GSPN reward models, *Performance Evaluation*, 1991, 12, 237–253.
4. MEYER, J. F. Closed form solutions of performability, *IEEE Trans.*, 1982, C-31, 648–657.

Thesis Abstract (M. Sc. (Engng))

An automatic parallelization framework for multi-computers by U. Nagaraj Shenoy

Research supervisor: Y. N. Srikant

Department: Computer Science and Automation

1. Introduction

Automatic parallelization is very important in the case of multi-computers because of the complexity of programming these machines and also because some way of reusing the huge amounts of software written for sequential machines is essential. Data partitioning has always been the major problem in automatic parallelization for this class of machines.

Earlier research^{1,2} in automatic data partitioning concentrated mostly on static data partitioning. Considering the advances in hardware technology in communication mechanisms, we feel that dynamic data partitioning and distribution is not only feasible, but may be more efficient on these machines.

2. Iteration space partitioning

Since the programs are known to spend major chunk of the time in executing loops, we look at loop-level parallelism. Also since multi-computers are most suitable for data parallel problems, we adopt an SPMD model. We employ a variation of

tiling transformation to achieve coarse grain parallelism. Based on the dependence vector for a loop nest, we categorize the loop nests into various classes, namely, *parallel partitionable*, *balanced subparallel partitionable* and *unbalanced sub-parallel partitionable*.

Example 1

```
do i = 1, N
  do j = 1, N
    C[i, j] = 0
    do k = 1, N
      C[i, j] = C[i, j] + A[i, k]*B[k, j]
    enddo
  enddo
enddo
```

This is a parallel partitionable loop nest. Loops I and J can be sectioned to result in P tiles where the tiles are independent of each other and hence each tile can be executed by one of the P processors. The partitioned loop nest is shown below.

```
do i = X*N/R + 1, X*N/R + N/R
  do j = Y*N/S + 1, Y*N/S + N/S
    C[i, j] = 0
    do k = 1, N
      C[i, j] = C[i, j] + A[i, k]*B[k, j]
    enddo
  enddo
enddo
```

where $X = p/R$ and $Y = \text{MOD}(p, R)$. p is the processor id.

Example 2

```
do i = 1, L
  do j = 1, M
    do k = 1, N
      A[i, j, k] = A[i-1, j-1, k-1] +
        A[i, j-4, k-2] + A[i, j, k-3]
    enddo
  enddo
enddo
```

This loop nest has no parallel partition but it can be partitioned in such a way that it results in groups of tiles where the tiles within a group are independent of each other and the groups themselves are executed one after the other. Since the outer loop is executed sequentially and needs explicit synchronization across processors, loop permutation helps in bringing the smallest loop out. One such partition is shown below.

```
do k = 1, N
  do i = p*L/P + 1, (p + 1)*L/P
    do j = 1, M
      A[i, j, k] = A[i-1, j-1, k-1] +
        A[i, j-4, k-2] + A[i, j, k-3]
    enddo
  enddo
enddo
```

Each tile group has the same number of tiles and hence we call this as balanced sub-parallel partition.

Example 3

```

do I = 1, N
  do J = 1, N
    G[I, J] = G[I-1, J] + G[I + 1, J] +
              G[I, J-1] + G[I, J + 1]
  enddo
enddo

```

This loop nest has neither parallel partition nor balanced sub-parallel partition. We partition the iteration space into T tiles and comb these tiles across P processors as follows.

```

k = SQRT(T)
sl = N/k
do ic = p, min(k-1, p + k), P
  do ip = 1, N, sl
    do i = ic + 1, ic + sl
      do j = ip, ip + sl-1
        A[i, j] = A[i-1, j] + A[i, j-1] +
                  A[i + 1, j] + A[i, j + 1]
      enddo
    enddo
  enddo
enddo

```

The tile groups have unequal number of tiles and the ordering of the tile groups takes place at runtime because of the data dependence.

All the above examples considered rectangular iteration spaces. In case the iteration space is not rectangular, we consider the inner loop nest which has a rectangular iteration space.

3. Data partitioning

After necessary transformations, we convert a sequential program into a sequence of program segments. There can be no communication in the middle of a segment. This implies that all the data required by a segment have to be locally available. The partitioning of the loop nest often implies partitioning of the associated arrays and each processor acquires the sections of the arrays corresponding to the part of the loop nest it executes.

We define a section as a portion of an array used by a segment. It comprises a collection of elements of the array. Different sections of an array may be accessed by different processors at different instances of time. The sections which are modified by a processor are said to be owned by that processor at that instant. A processor may just refer to a section without modifying it. Such sections are said to be used by that processor. An used section is *read only* and hence can be replicated on all the processors if needed.

Table I

mat	proc0	proc1	proc2	proc3
A	$x_{1, \frac{N}{2}}$	$x_{1, \frac{N}{2}}$	$x_{\frac{N}{2}+1, N}$	$x_{\frac{N}{2}+1, N}$
	$y_{1, N}$	$y_{1, N}$	$y_{1, N}$	$y_{1, N}$
B	$x_{1, N}$	$x_{1, N}$	$x_{1, N}$	$x_{1, N}$
	$y_{1, \frac{N}{2}}$	$y_{\frac{N}{2}+1, N}$	$y_{1, \frac{N}{2}}$	$y_{\frac{N}{2}+1, N}$
C	$x_{1, \frac{N}{2}}$	$x_{1, \frac{N}{2}}$	$x_{\frac{N}{2}+1, N}$	$x_{\frac{N}{2}+1, N}$
	$y_{1, \frac{N}{2}}$	$y_{\frac{N}{2}+1, N}$	$y_{1, \frac{N}{2}}$	$y_{\frac{N}{2}+1, N}$

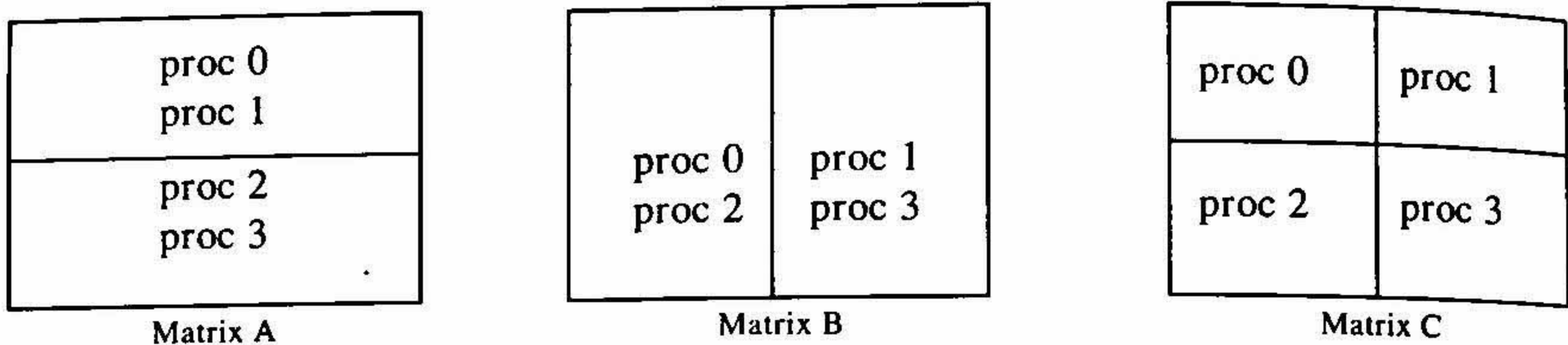


FIG. 1.

The array elements which appear on the left-hand side of an assignment statement form part of the section owned by the processor executing the set of statements, whereas those appearing on the right-hand side form the used section. Each array reference along with corresponding subscript functions gives rise to a part of a section of that array. Sections are described by *index generating functions* (IGF). An IGF for a section is a function which generates indices of all its elements.

We define various operations on index-generating functions like union, intersection, difference, approximation and reduction. These operations are very useful in the runtime management of the sections. The IGF, for example, 1, assuming $P = 4$, $R = S = 2$, are shown in Table I. Each function is of the form $f(x, y) = \langle x, y \rangle$, x and y bounded as shown. The actual data partition is shown in Fig. 1. Array \mathcal{A} is partitioned into strips of consecutive rows, array \mathcal{B} is partitioned into strips of consecutive columns and the array \mathcal{C} is block partitioned. Also, observe that various sections of the arrays are properly aligned with respect to each other. Parts of both matrices, \mathcal{A} and \mathcal{B} , are replicated.

4. Runtime management of sections

Sectioning of the arrays is done dynamically and these sections are moved across processors as and when required. Our model assumes a runtime system which implements a *sectioned distributed shared memory* (SDSM), which does most of the runtime management of the sections. The basic task involves re-partitioning of the arrays into sections as required by the current segment, redistributing the sections to the desired processors and maintaining data consistency. Before the beginning of every segment, the runtime system ensures that the data required by each processor resides in its local memory.

The local memory of a processor acts like a *section cache* from which the sections needed by the current segment are accessed. The effectiveness of any cache depends on the access pattern and the locality of reference. We believe that any large program exhibits sufficient amount of locality of reference.

There is a high probability that the sections acquired by a segment are going to be re-used several times, both by the segment which has acquired them and also by the segments which follow, before the sections get re-partitioned/redistributed. Also, it is possible to prefetch sections required for succeeding sections, in parallel with the execution of the current section, without interfering with the currently fetched sections. This effectively overlaps computation of the current segment with the communication involved in the prefetch. In ideal situations prefetch should result in negligibly small redistribution overheads.

5. Case studies

We have taken a couple of simple program fragments, each representative of various types of loop nests discussed in Section 2. The transformed program is run on PARAM, a 256-node multicomputer developed at C-DAC³.

Table II
Concatenated matrix multiplication

# Processors	Speed up	Efficiency (%)
4	3.5	89.5
8	6.8	85.0
16	11.6	72.3

Table III
Successive overrelaxation (SOR)

# Processors	Speed up	Efficiency (%)
4	3.63	90.8
8	6.12	76.5
16	8.79	54.9

Table IV
Gaussian elimination

# Processors	Speed up	Efficiency (%)
4	3.9	97.5
8	6.57	82.1
12	7.51	62.6

6. Conclusions

In this paper we propose a coherent framework for automatic parallelization of sequential programs for distributed memory message passing class of multiprocessors. The framework covers most of the issues involved in automatic parallelization. Issue specific to multicomputers, namely, data partitioning is handled by resorting to automatic detection of partitions using index-generating functions and dynamically distributing the data with the help of a runtime system which gives an illusion of a sectioned distributed shared memory.

We have concentrated mostly on loop-level parallelism where we classify the loop nests into various cases and handle each in a specific way. There are still loops like those with arbitrary dependence vectors which are not handled by our scheme. We have also not looked into task- or procedure-level parallelism. We these to future work.

References

1. MANISH GUPTA AND PRITHVIRAJ BANERJEE
Demonstration of automatic data partitioning techniques for parallelizing compilers on multicomputer, *IEEE Trans.* 1992, PDS-3, 179-193.
2. RAMANUJAM, J. AND SADAYAPPAN, P.
Compile-time techniques for data distribution in distributed memory machine, *IEEE Trans.*, 1991, PDS-2, 472-482.
3. P. R. EKNATH, *et al.*
Param parallel computer. Advanced computing, Tata McGraw-Hill, 1991.

Thesis Abstract (M. Sc. (Engng))

Vibration of pipes resting on soil medium by S. Raghava Chary

Research supervisors: R. N. Iyengar and C. Kameswara Rao (BHEL)

Department: Civil Engineering

1. Introduction

Pipelines are used extensively for transportation of fluids. Fluid velocity which depends on the intended purpose, imparts energy to the pipe making it to vibrate. Apart from this, pipes are supported in many ways. While indoor piping is supported on structures, cross-country pipelines used for transporting petroleum products are either laid on ground or buried. Good amount of literature is available in the area of pipes conveying fluid with emphasis on stability aspects addressing critical flow velocities¹⁻³. However, the problem of pipe conveying fluid resting on elastic medium has not been fully understood. A modest attempt is made in this thesis to present an approximate analysis for the problem of pipe conveying fluid resting on an elastic medium. In addition, the studies made in the area of a beam on elastic foundation closely representing the situation of a pipe on soil medium is presented.

2. Free vibration analysis

In the first place the soil is modelled as a Winkler foundation. Considering the case of a single span pipe resting on Winkler-type elastic medium, free vibration analysis is carried out. Equations are obtained for the fundamental

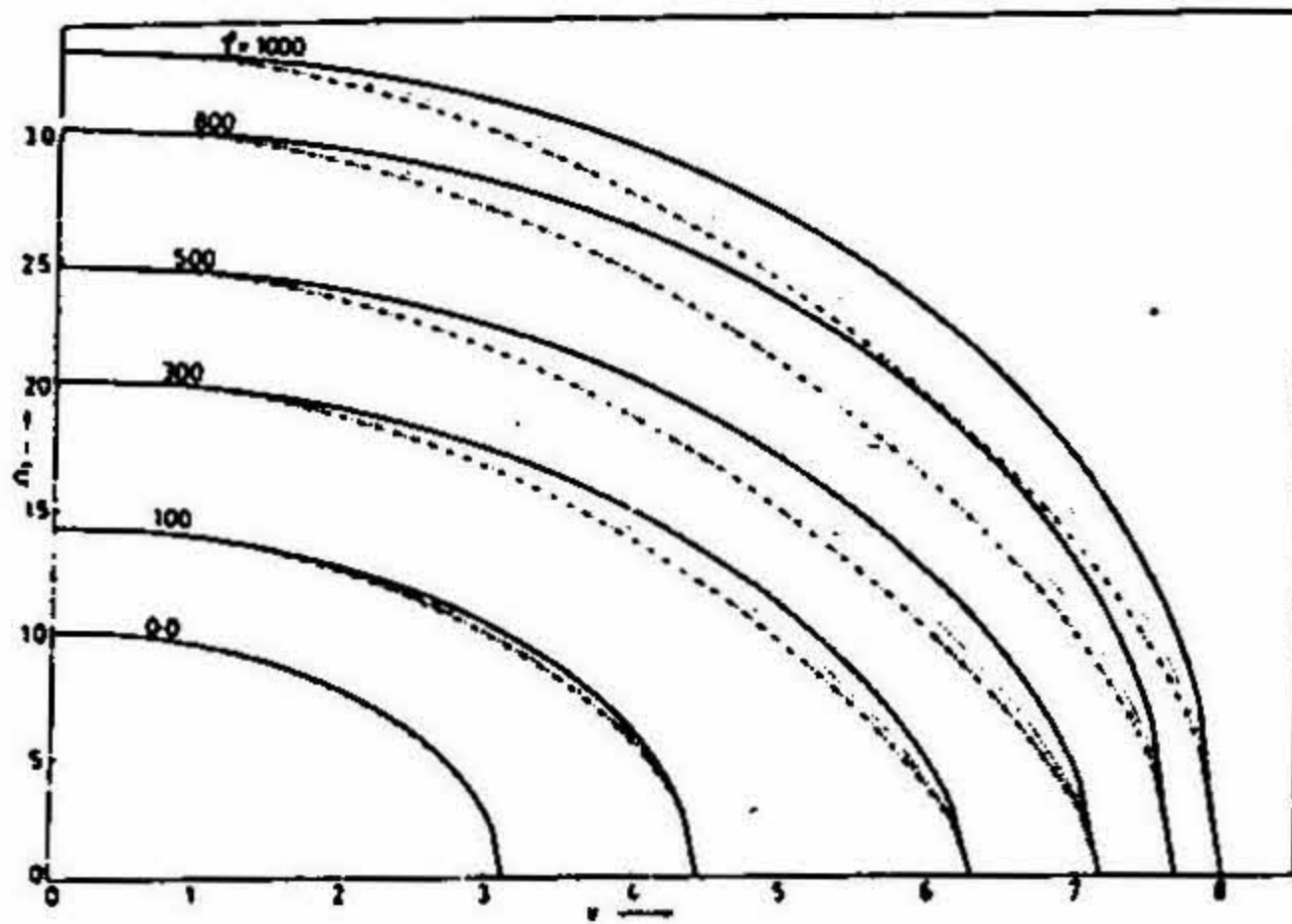


FIG. 1. Effect of V on Ω_1 for hinged-hinged pipe for various values of γ . — $\beta = 0.3$; $\beta = 0.6$ and — · — $\beta = 0.7848$.

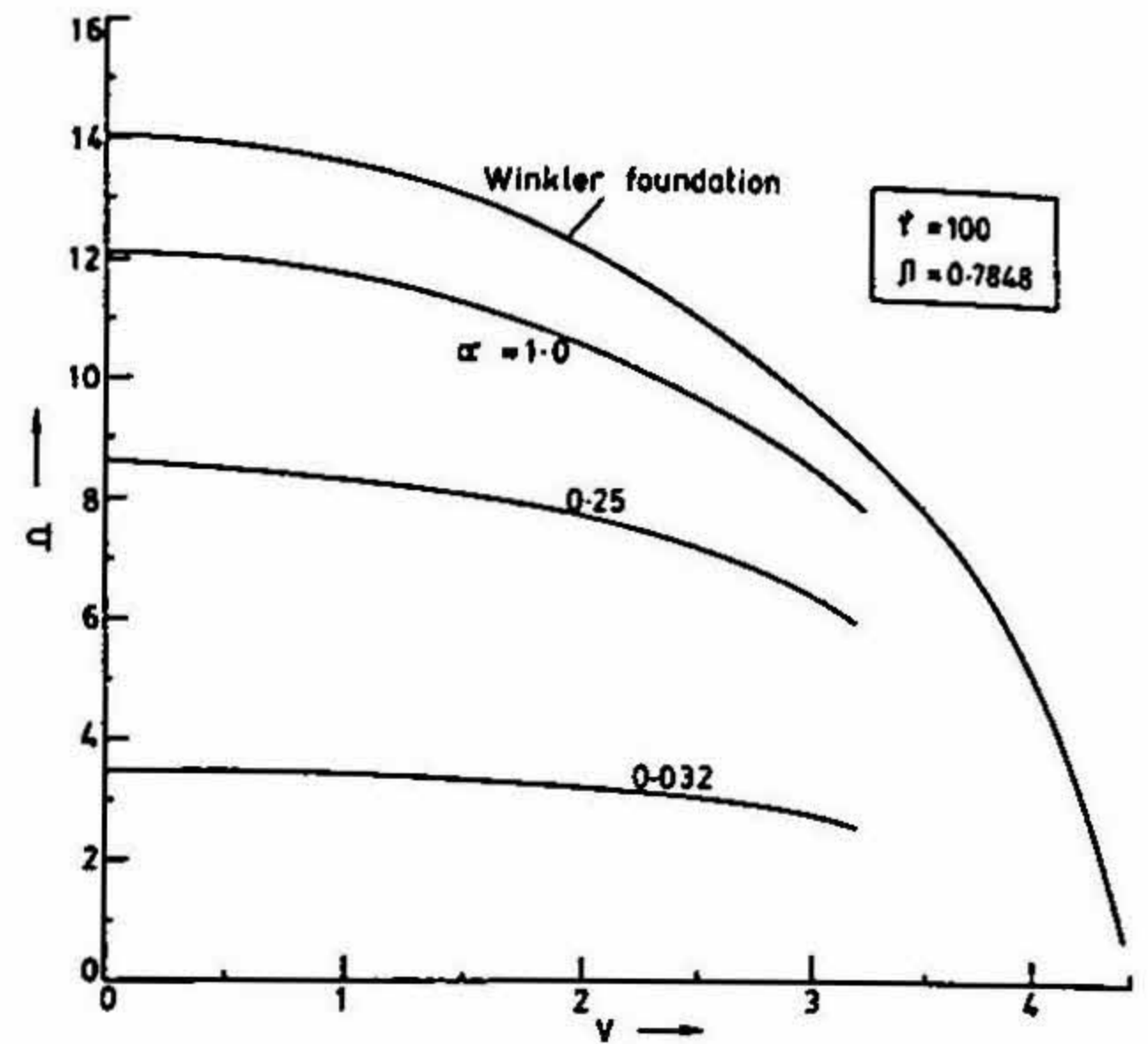


FIG. 2. Effect of α on Ω . Hinged-hinged pipe. $\gamma = 100$ and $\beta = 0.7848$.

frequency parameter and the critical flow velocity flow velocity parameter for various values of foundation stiffness parameter and mass ratio parameter. Three types of boundary conditions, namely, hinged-hinged, fixed-hinged and fixed-fixed are considered for investigation. Results are presented graphically showing the variation of fundamental frequency parameter for increasing values of mass ratio, flow velocity and foundation parameters. Figure 1 shows the effect of increase in flow velocity parameter V on the fundamental frequency parameter Ω for various values of mass ratio parameter β and foundation stiffness parameter γ .

The above model is improved to include the foundation inertia. In this case, the soil is modelled as a series of vertically vibrating independent bars fixed at the bottom and connected to the pipe at the top. Corresponding frequency equations are obtained for three boundary conditions considered. These equations are transcendental in nature and are solved using bisection method. Numerical results are obtained to show the variation of fundamental natural frequency parameter Ω with the flow velocity parameter V and the foundation mass parameter α . Figure 2 shows a comparison of values of frequency parameter obtained using Winkler model and the improved model including foundation inertia.

3. Forced vibration response

In many situations, the transportation pipelines carrying important fluids such as petroleum products are designed against earthquake loading. The presence of Coriolis term makes this problem more complex and the usual normal mode approach cannot be applied directly. Considering the case of pipelines with low flow velocity (< 25 m/s), the effect of Coriolis term on the fundamental frequency is studied and found to be negligible. A restricted analysis for seismic response of pipes ignoring Coriolis term is attempted. Response for a typical pipeline with hinged-hinged end condition using both the response spectrum method and the time history analysis is obtained for the vertical component of Taft 1952 earthquake.

4. Conclusions

1. For any particular value of the foundation stiffness, it is observed that the fundamental natural frequency of the pipe decreases significantly for increase in value of flow velocity (For a typical value of $V = 3$, reduction in Ω is 30%).

2. Study using finite depth foundation model showed⁴ that the effect of foundation inertia on the fundamental natural frequency is quite significant (up to a maximum of 50%) and hence cannot be ignored.

3. The frequency equations derived for various boundary conditions and pipe soil parameters can be appropriately used in design.

References

1. BLEVINS, R. D. *Flow-induced vibration*, 1977, Van Nostrand-Reinhold.
2. DERMENDJIAN-IVANOVA, D. S. Critical flow velocities of a simply-supported pipeline on an elastic foundation, *J. Sound Vibration*, 1992, 157, 370–374.
3. HOUSNER, G. W. Bending vibrations of a pipe when liquid flows through it, *J. Appl. Mech.*, 1952, 19, 205–208.
4. IYENGAR, R. N. AND PRANESH, M. R. Dynamic response of a beam on a foundation of finite depth, *Indian Geotech. J.*, 1985, 15, 53–63.

Thesis Abstract (M. Sc. (Engng))

Assessment of shell theories for the static analysis of laminated circular cylindrical shells by D. V. T. G. Pavan Kumar

Research supervisor: K. Chandrashekhara

Department: Civil Engineering

1. Introduction

Analysis of composite material shell structures has been of considerable research interest because of increasing use of high-performance fiber-reinforced laminated shell structures in various fields of modern technology like aeronautical, civil, marine, mechanical, nuclear and automobile engineering. In laminated shell structures, the finite length laminated circular cylindrical shell has received wide attention.

Many classical shell theories are available in literature to analyse the laminated circular cylindrical shell of revolution and shell panel. Originally, many classical shell theories have been developed based on Kirchhoff–Love hypothesis to analyse thin isotropic shell structures. Many investigators have extended these classical shell theories to laminated shell structures, sometimes incorporating first and higher-order shear deformation effects for better prediction of behaviour under static, dynamic and buckling loads.

Shell theories that have been often used in the analysis of laminated circular cylindrical shells are those given by Flugge, Sanders, Love and Donnell and hence in the present study, these classical shell theories (CST) have been chosen. The present study deals with static response of laminated circular cylindrical shell of revolution and shell panel by using all the afore-mentioned shell theories. The main objectives of the present study are: (1) to assess the accuracy of the afore-mentioned classical shell theories in the light of available three-dimensional elasticity solution for simply supported circular cylindrical shells, (2) to examine the effect of incorporation of first-order shear deformation (FSDT) over all the afore-mentioned classical shell theories, (3) to establish the range of applicability of the shell theories, specifically from the point of design keeping in view the lamination schemes, boundary conditions, and geometrical parameters like length-to-radius and thickness-to-radius of the shell.

2. Static analysis of laminated circular cylindrical shells

Detailed literature survey on analytical approaches available for the analysis of laminated circular cylindrical shells has been presented very systematically. The basic equations (equilibrium equations, strain-displacement relations and force-displacement relations), for the static analysis of laminated circular cylindrical shells corresponding to the afore-mentioned shell theories (CST and FSDT) have been presented in a unified form by using tracer coefficients. The basic equations corresponding to the theories (CST and FSDT) of Flugge, Sanders, Love and Donnell could be obtained by using appropriate tracer coefficients. The basic equations of membrane theory have also been presented for the static analysis of cross-ply laminated circular cylindrical shells.

2.1. Navier-type solution

Navier-type solution has been utilised to analyse the simply supported shell of revolution and an all-round simply supported shell panel, by using both CST and FSDT. Assessment of the afore-mentioned classical shell theories has been made in comparison with available three-dimensional elasticity solution¹ and conclusions have been drawn keeping in view the geometrical parameters like length-to-radius and thickness-to-radius ratios of the shell and various lamination schemes. A study has also been made to examine to what extent FSDT improves the results over CST. For this purpose, cross-ply laminated circular cylindrical shell, made up of high-modulus graphite-epoxy, has been considered.

2.2. Levy-type solution

In literature, for laminated circular cylindrical shells, Levy-type solution has been developed by Khdeir *et al.*² by using state-space technique. In the present study, a simple and direct procedure, similar to the procedure given by Flugge³ for isotropic shells, has been extended to obtain a Levy-type solution for cross-ply laminated circular cylindrical shell of revolution and shell panel using all afore-mentioned classical shell theories. Detailed numerical results have been presented for different lamination schemes, boundary conditions, loads and geometric parameters like length-to-radius and thickness-to-radius ratios of the shell. For some typical cases, the results of present solution have been compared with the available results in the literature. Comparisons have also been made between the afore-mentioned classical shell theories.

2.3. Galerkin method

Galerkin method has been adopted to analyse an all round clamped cross- and angle-ply laminated circular cylindrical shell panels as well as circular cylindrical shell of revolution using the afore-mentioned classical shell theories. Beam functions and trigonometric functions have been assumed to satisfy the clamped boundary conditions. Results obtained from the present solution have been compared with some available finite element results in the literature. Parametric study has been carried out and comparisons have been made between the afore-mentioned classical shell theories.

3. Conclusions

Classical shell theories according to Flugge, Sanders and Love are equally good in predicting the results for all length-to-radius (L/R) ratios, lamination schemes and boundary conditions. In general, all classical shell theories (CST) underpredict the radial displacements. First-order shear deformation theories (FSDT) give considerable amount of improvement in predicting the results for $L/R = 0.5$ while for $L/R \geq 2$ the improvement is marginal for radial displacement and inconsistent in the case of longitudinal and circumferential stresses. Donnell's theory gives erroneous results for circumferential stress for $L/R > 1$ in the case of 90° ply shell of revolution and in the case of laminated shell of revolution having more number of 90° plies and less predominant in the presence of more number of 0° plies. In general, Donnell's shell theory gives erroneous results for long shells (both shell of revolution and shell panel) and hence it is not recommended for $L/R > 1$. Laminated circular cylindrical shell panel needs less length to attain plane strain condition if it contains more number of 90° plies and more length if it contains less number of 90° plies. Incorporation of higher-order shear deformation over accurate theory like Flugge's shell theory gives better results than an approximate theory like Donnell's shell theory.

References

1. SREEHARI KUMAR, B. *Analysis of thick orthotropic and laminated circular cylindrical shells*, Ph. D. Thesis, Civil Engineering Department, Indian Institute of Science, Bangalore, India, 1992.
2. KHDEIR, A. A., REDDY, J. N. AND FREDERICK, D. A study of bending, vibration, and buckling of cross-ply circular cylindrical shells with various shell theories, *Int. J. Engng Sci.*, 1989, 27, 1337-1351.
3. FLUGGE, W. *Stresses in shells*, second edn, 1973, Springer.

Thesis Abstract (M. Sc. (Engng))

Heat and mass transfer simulation studies in solid state fermentations by S. Rajagopalan

Research supervisor: Jayant M. Modak

Department: Chemical Engineering

1. Introduction

Solid state fermentation (SSF) processes have long been employed in the production and preservation of a variety of foods, and in the production of enzymes, organic acids, antibiotics and other microbial products. They are fermentation processes that take place due to the action of microorganisms on solid or semisolid substrates. The substrate is a nutritionally inert solid support, whose presence is advantageous to the microorganisms with respect to access to nutrients¹. Certain SSF products are used as foods, and the texture developed during fermentation is an important attribute of the product. Static tray fermenter is one of the types of fermenters used in producing food products of desired quality. Major problems in SSF fermenters in general and static bed fermenters in particular are heat build up and oxygen diffusional limitations². A detailed knowledge of the interrelationship of heat and mass transfer is essential for the rational design and control of SSF processes. In the present investigation, experiments have been conducted to understand fungal growth on solid substrates and models have been proposed to understand heat and mass transport and cell growth.

2. Present work

Experiments were conducted in shake flasks as well as in a Perspex tray fermenter to understand the fungal growth on wheat bran as the solid substrate. The organism used in the study is *Aspergillus niger*.

The shake flask experiments revealed that the fungi formed a white mat around individual bran particles and also that enough pore space is needed for the fungi to penetrate through the substrate matrix. The observation of the growth around individual particles showed that the fungi formed a thin sheath around the particles and the thickness of this thin layer or the fungal biofilm is not constant with time. The tray experiments showed that after the completion of fermentation the brain shrunk in volume and became a cake thereby leaving space between the walls of the fermenter and the cake. The temperature profiles were measured with thermocouples and it was observed that there was a period of constant increase in temperature followed by a steady period and the temperature values dropped once the fermentation was over.

In the modelling aspect of the work, first a pseudo-homogeneous model was proposed. The pseudo-homogeneous model considered a biofilm on individual substrate particles. A pseudo-steady state was assumed between the oxygen transfer on to the film surface and the subsequent consumption by cells. Oxygen was assumed to be growth limiting and the consumption of oxygen was assumed to follow Monod's kinetics. Mass balance and heat balance equations representing the transport processes taking place in the fermenter were written based on the typical tray fermenter system used for experiments by earlier workers³. The resulting partial differential equations were solved using orthogonal collocation. The model predictions were compared with the available data in the literature³ and they agree qualitatively well with the experimental trends. The effect of variation of several operational parameters like the flow rate of gas, incubation temperature, initial inoculum size, substrate thickness, initial oxygen concentration and the porosity of the bed on the performance of the fermenter was studied. It was found that the incubation temperature and the substrate thickness had profound effect on the yield from the fermenter whereas the other parameters did not have much effect. It was also found that the performance of the fermenter open at both ends was better than that of the fermenter closed at the bottom. Simulations were done to find optimal incubation temperature and substrate thickness values for the maximum cell mass yield from the fermenter.

Based on the experimental observation of the expanding biofilm around the individual wheat-brain particles, a heterogeneous model was proposed which considered the reduction in porosity and increase in oxygen diffusion resistance due to such biofilm growth. Steric hindrance limitation reported in the literature⁴ was also incorporated into the model. The moving boundary of the biofilm was immobilised using a suitable transformation and the pertinent partial differential equations were solved using orthogonal collocation technique. The theoretical pre-

diction on the maximum possible utilization of the available space for cell growth was incorporated⁴ and the effect of variation of some intrinsic parameters like maximum growth rate of the organism, thermal conductivity, heat of the reaction, heat capacity of the substrate and the radius of the particle were studied. It was also found that the heterogeneous model compared with the pseudo-homogeneous model at the limiting conditions of high cell density and low oxygen diffusivity of oxygen through the biofilm.

Finally, glucose limitation on the cell growth was studied, by proposing a model for a single particle system, following the earlier work reported in the literature⁵. The conclusion from the results of the model on single particle system was that glucose does act as a growth-limiting substrate. Oxygen limitation on growth was imposed on the single particle system by assuming oxygen to be present at constant concentration level at the boundary. It was observed that oxygen limitation on growth was more pronounced than glucose limitation. Glucose became growth limiting only during the later stages of fermentation and the fermentation time during which glucose became growth limiting decreased as the value of the concentration of the film phase oxygen assumed to be present at the boundary of the biofilm was decreased. To check the validity of these conclusions in the actual fermenter, a unified model has been proposed, combining the characteristic features of the heterogeneous model and the single particle substrate model. It has been found from this unified model that oxygen is more severely growth limiting than glucose, and in the presence of oxygen limitation, glucose does not limit the cell growth process. It was also found that the cell mass yield from the fermenter with and without the presence of glucose limitation was the same implying that in the presence of oxygen as the growth-limiting factor, glucose limitation was negligible. It is hoped that the mathematical models developed will help in a better understanding of the transport processes involved and thus improve the design of the fermenter and the control of the fermentation process.

References

1. HESSELTINE, C. W. Solid state fermentations, *Biotechnol. Bioengng*, 1972, 14, 517-532.
2. LONSANE, B. K., GHILDYAL, N. P., BUDIATMAN, S. AND RAMAKRISHNA, S. V. Engineering aspects of solid state fermentation, *Enzyme Microb. Technol.*, 1985, 7, 258-265.
3. RATHBUN, B. L. AND SHULER, M. L. Heat and mass transfer effects in static solid-substrate fermentations: Design of fermentation chambers, *Biotechnol. Bioengng*, 1983, 25, 929-937.
4. LAUKEVICS, J. J., ASPITE, A. F., VIESTURS, U. S. AND TENDERDY, R. P. Steric hindrance of growth of filamentous fungi in solid substrate fermentation of wheat straw, *Biotechnol. Bioengng*, 1985, 27, 1687-1691.
5. MITCHELL, D. A., DO, D. D., GREENFIELD, P. F. AND DOELLE, H. W. A semimechanistic mathematical model for growth of *Rhizopus oligosporus* in a model solid state fermentation system, *Biotechnol. Bioengng*, 1991, 38, 353-362.

Thesis Abstract (Ph. D.)

The mechanism of interaction of carbonyl-directed reagents at the active site of sheep liver serine hydroxymethyltransferase by Jairaj Kumar Acharya

Research supervisor: N. Appaji Rao

Department: Biochemistry

1. Introduction

Serine hydroxymethyltransferase (SHMT E. C. 2. 1. 2. 1) is an important enzyme in the pathway for the biosynthesis of nucleotides and amino acids. Although extensive studies have been carried out on this enzyme from a variety of sources, clinically effective inhibitors of this enzyme are not yet available¹. The study on the interactions of O-amino-D-serine (OADS) and aminooxyacetic acid (AAA) with sheep-liver SHMT had indicated that

they were effective inhibitors of the enzyme^{2,3}. It was therefore of importance to elucidate the minimal structural requirement for the unique interaction of aminoxy compounds with this enzyme. It was also of interest to elucidate the mechanism of interaction of the more reactive hydrazides such as thiosemicarbazide, semicarbazide and other substituted thiosemicarbazides with the enzyme.

2. Experimental

SHMT was purified in large amounts and to homogeneity. The mechanism of interaction of methoxyamine, thiosemicarbazide, semicarbazide and substituted thiosemicarbazide was studied by spectral measurements including circular dichroism, fluorescence, stopped-flow spectrophotometry and using separation techniques such as HPLC and centricon filtrations.

3. Results and discussion

3.1. Interaction of methoxyamine with SHMT

It was established that the mechanism of interaction of methoxyamine with the enzyme was similar to that of OADS and aminoxyacetic acid. However, the reaction with AAA was about two orders of magnitude faster than methoxyamine in the initial phase of interaction with the enzyme. These results highlighted the importance of the carboxyl group in enhancing the reactivity of substituted aminoxy compounds⁴.

3.2. Interaction of L-cycloserine and serine hydrazides with SHMT

A preliminary examination of the interaction of L-cycloserine (LCS) with the enzyme revealed that LCS inhibited the enzyme in a time and concentration-dependent manner. The spectral features and the inhibition studies indicated that LCS inhibited the enzyme by a mechanism similar to that of D-cycloserine⁵.

Studies with L- and D-serine hydrazides revealed that the former was a more potent inhibitor of the enzyme.

3.3. Inhibition of SMHT by thiosemicarbazide

Thiosemicarbazide (TSC) inhibited the enzyme in a time-dependent biphasic manner. Spectral studies indicated that the interaction of TSC with the enzyme resulted in the formation of a unique intermediate absorbing at 464 and 440 nm. This intermediate was generated at the active site of the enzyme and remained bound to it. The intermediate was converted very slowly to the product PLP-thiosemicarbazone. The interaction of formaldehyde with the intermediate suggested that it could be a resonance-stabilized intermediate⁶.

3.4. Interaction of semicarbazide and substituted thiosemicarbazides with SHMT

Semicarbazide(SC) was found to be a potent inhibitor of the enzyme and this interaction generated a short-lived intermediate. Aminoguanidine and 2-methyl-thiosemicarbazide were poor inhibitors of the enzyme. The interaction of 4-methyl-thiosemicarbazide with the enzyme was similar to that of thiosemicarbazide but was less effective. Thiocarbohydrazide was the most potent inhibitor of all the hydrazides studied. It was thus demonstrated that substitutions which interfere with the formation of a resonance-stabilized structure involving the 2-nitrogen and 3-thioketone interfered with the efficacy of interaction of the compound with the enzyme. A minimal kinetic mechanism was proposed for the unique interaction of thiosemicarbazide with sheep-liver SHMT.

References

1. APPAJI RAO, N. *New trends in biological chemistry* (Ozawa, T., ed.) pp. 333-340, 1991, Japan Scientific Press, Tokyo.
2. BASKARAN, N. *et al.* *Biochemistry*, 1989, 28, 9607-9612.
3. BASKARAN, N. *et al.* *Biochemistry*, 1989, 28, 9613-9617.
4. ACHARYA, J. K. *et al.* *Indian J. Biochem. Biophys.*, 1991, 28, 381-388.

5. MANOHAR, R. *et al.* *Biochemistry*, 1984, 23, 4116–4122.
6. ACHARYA, J. K. AND APPAJI RAO, N. *J. Biol. Chem.*, 1992, 267, 19066–19071.

Thesis Abstract (Ph. D.)

The primary structure and active site residues of sheep liver hydroxymethyltransferase by Usha Rajagopalan

Research supervisor: N. Appaji Rao

Department: Biochemistry

1. Introduction

Serine hydromethyltransferase (SHMT E. C. 2. 1. 2. 1) is a unique PLP-enzyme catalyzing the hydroxymethyl-transfer from serine to tetrahydrofolate (H_4 -folate)¹. SHMT, in addition to its special position in the pyridoxal-5'-phosphate (PLP) group of enzymes, is part of the thymidylate cycle along with dihydrofolate reductase (DHFR) and thymidylate synthase (TS). Extensive structural studies (primary as well as X-ray crystallographic structures) have been carried out on DHFR and TS while such structural studies on SHMT were minimal^{2,3}. It was therefore important to elucidate the primary structure of sheep-liver SHMT as this would lead to a better understanding of the structure–function relationship in SHMT and other PLP enzymes. It was also of interest to identify active site residues that would help in understanding the mechanism of action of the enzyme and lead to the design of inhibitors for the enzyme.

2. Experimental

Sheep-liver SHMT was purified to homogeneity. SHMT was cleaved by enzymatic and chemical methods. Peptides were isolated by RP-HPLC and electrophoretic separation. Manual sequencing was carried out by the DABITC/PITC double-coupling method⁴ and automated sequencing using a gas-phase sequenator.

3. Results and discussion

3.1. Purification and sequencing of peptides from enzymatic cleavages of SHMT

Three differently pretreated SHMTs were used for tryptic cleavage (a) reduced, carboxymethylated SHMT⁴, (b) performic acid oxidized SHMT, (c) [¹⁴C]-iodoacetic acid (IAA)-labeled SHMT. The first digest provided the tryptic peptides which formed the framework for the elucidation of the complete sequence. The peptides from the second digest were useful in obtaining long sequences and the third digest aided in identifying Cys peptides. The chymotryptic digest of SHMT was useful mainly in confirming the earlier tryptic sequences.

3.2. Purification and sequencing of peptides obtained upon chemical cleavage of SHMT

The separation of CNBr peptides by tricine gel electrophoresis followed by electroblotting on to PVDF membrane and direct sequencing of the blots provided long stretches of sequences and overlaps to tryptic peptides. Chemical cleavage of SHMT by hydroxylamine proved useful in the identification of the blocked N-terminal peptide.

3.3. Construction and analysis of the primary structure of sheep-liver SHMT

The comparison of primary structure of sheep-liver SHMT consisting of 483 amino acids was obtained by aligning the tryptic, chymotryptic, CNBr and hydroxylamine peptides. The validity of the sequence determined was established by amino acid composition determined by acid hydrolysis and the composition of the protein deduced from the sequence.

A comparison of the sequence of sheep-liver SHMT with other known SHMT sequences revealed a high degree of conservation among SHMTs. An alignment of the SHMT sequence with other PLP enzymes revealed no

significant homology in primary structure. However, PLP enzymes revealed the presence of alternating helices and strands in several of them. The hydrophathy plots for SHMTs were also similar.

3.4. Identification of active site residues of SHMT

Earlier work from this laboratory showed that Arg, His, Cys and Lys residues were essential for the activity of SHMT. The Lys residue involved in the formation of the internal aldimine with PLP was identified by reducing the enzyme with sodium borohydride. The PLP peptide was isolated by monitoring its characteristic fluorescence and sequenced. The decapeptide-binding PLP was identical in several SHMT sequences indicating the importance of this region in binding or catalysis.

The incorporation of [^{14}C]-PG indicated that two Arg residues were modified per subunit of the enzyme and the modification of these residues was prevented by H_4 -folate. In order to locate the sites of PG modification, SHMT was reacted with unlabeled PG in the presence of H_4 -folate followed by radioactive PG in the absence of H_4 -folate. Tryptic cleavage of the labeled PG-treated enzyme followed by isolation and sequencing of the radiolabeled peptides indicated that Arg-269 and -462 were the sites of PG modification. Neither a spectrally discernible quinonoid intermediate (characteristic of the native enzyme when substrates are added) nor its enhancement by the addition of H_4 -folate was observed with the PG-modified enzyme. There was no enhancement of the rate of the exchange of the α -proton of Gly upon addition of H_4 -folate to the modified enzyme as was observed with the native enzyme⁶. Two Cys residues, Cys-67 and -203, were protected by PLP and were isolated by the use of [^{14}C]-IAA for carboxymethylation followed by tryptic digestion of the holo- and apo-enzymes. The conformationally buried Cys residues were also identified by comparing the radiolabeled tryptic peptides obtained from the native and denatured enzyme.

Thus the elucidation of the primary structure of sheep-liver SHMT and identification of some active site residues should aid in the understanding of the structure-function relationships among SHMTs and PLP enzymes.

References

1. APPAJI RAO, N. *New trends in biological chemistry*, (Ozawa, T., ed.) pp. 333-340, 1991, Japan Sci. Soc. Press, Tokyo.
2. MARTINI, F. *et al.* *J. Biol. Chem.*, 1987, 262, 5499-5509.
3. MARTINI, F. *et al.* *J. Biol. Chem.*, 1989, 264, 8509-8519.
4. CHANG, J. Y. *et al.* *FEBS Lett.*, 1978, 93, 205-214.
5. USHA, R. *et al.* *Indian J. Biochem. Biophys.*, 1992, 29, 183-188.
6. USHA, R. *et al.* *J. Biol. Chem.*, 1992, 267, 9289-9293.

Thesis Abstract (Ph. D.)

Mapping of antigenic determinants and regions of RNA-protein interactions in *Physalis mottle virus* by Ramesh Kekuda

Research supervisors: H. S. Savithri and A. Anjali Karande

Department: Biochemistry

1. Introduction

Physalis mottle virus (PhMV), a member of the tymovirus group, is an icosahedral virus infecting mainly Solanaceae plants causing systemic mottling symptoms¹. The capsid structure of PhMV is formed of 180 coat protein subunits of molecular weight 20,000, encapsidating the genomic RNA. Although turnip yellow mosaic virus (TYMV), the type member of the tymo group of plant viruses, was one of the first viruses to be crystallized², no information is available on the three-dimensional structure of this or any other tymovirus. In the present thesis, the architecture of PhMV was investigated by cross-linking studies and epitope mapping using monoclonal antibodies.

2. Experimental

Polyclonal and monoclonal antibodies were raised against PhMV and its coat protein. Epitope mapping was performed using the peptides purified from enzymatically and chemically cleaved coat protein by different techniques such as ELISA, dot-blot and immunoblots. The immunoreactive peptides were sequenced by using a gas-phase automated sequencer. Region of RNA-protein interaction was identified after ultraviolet irradiation and isolation of the cross-linked peptide. PCR-amplified coat protein gene of PhMV was cloned into a suitable vector and expressed in *E. coli*.

3. Results and discussion

3.1. Characterization of polyclonal and IgM monoclonal antibodies to PhMV

Polyclonal antibodies were raised against PhMV and its coat protein and they were characterized. Monoclonal antibodies were raised against the coat protein by a rapid *in vitro* immunization protocol. Both the polyclonal and monoclonal antibodies obtained in this study recognized mainly surface epitopes³, which could be due to the highly hydrophobic nature of the coat protein, which would make the alternative conformations available for the protein in native as well as in the denatured state limited.

3.2. Architecture of PhMV as probed by monoclonal antibodies obtained after *in vivo* immunization

Five monoclonal antibodies were raised against the intact virus and three against the denatured coat protein by the classical immunization protocol, followed by fusion of splenocytes with myeloma cells. All these monoclonal antibodies recognized surface epitopes, since they were reactive both with the native virus as well as the denatured coat protein. Immunoreactivity of the purified peptides obtained after CNBr, trypsin, clostripain, V-8 protease digestion and a recombinant coat protein with a truncation of 21 residues at the N-terminus with various monoclonal antibodies enabled identification of two epitopes, one in the region of residues 22–36 and the other at 75–110⁶.

3.3. Cross-linking studies on PhMV

PhMV RNA was cross-linked to the coat protein by ultraviolet irradiation *in situ*. The isolated coat protein together with the linked RNA was digested with trypsin and the peptides were separated on high-performance liquid chromatography (HPLC). The peaks were monitored at 225 and 260 nm to identify the oligonucleotide-linked peptide. The cross-linked peptide was subjected to sequencing and a Val-Lys dipeptide was identified⁴. A cross-linking between the cytosine nucleus of RNA and Lys-10 of the coat protein was proposed⁴⁻⁷.

Structure of PhMV was shown to be similar to southern bean mosaic virus⁸ (SBMV) in terms of particle size, triangulation number and morphology⁹. Based on the immunological and cross-linking studies, we have proposed that the epitopic region 22–30 would correspond to the β C strand of SBMV and the region 1–21 encompassing the Lys-10 could correspond to the β A and β B strands of SBMV which are buried.

3.4. Expression of PCR-amplified coat protein gene of PhMV

The viral capsids of the tymoviruses are mainly stabilized by protein-protein interactions and only drastic conditions can disrupt them which results in the denaturation of the coat protein. In an attempt to obtain the native coat protein, coat protein gene was amplified using sense and antisense primers and the resultant product was cloned into an expression vector. When this clone was induced with 500 μ M IPTG for 10 h, an optimum expression of the protein was observed. This clone provides a good tool for future studies on the assembly of this virus and site-directed mutagenesis of the residues that are important in protein-protein and protein-RNA interactions.

References

1. SMITH, K. W. *Parasitology*, 1943, 35, 159–161.
2. KLUG, A., LONGLEY, W. AND LEBERMAN, R. *J. Mol. Biol.*, 1966, 15, 315–343.

3. KEKUDA, R., KARANDE, A. A. AND SAVITHRI, H. S. *Indian J. Biophys. Biochem.*, 1993, 30, 151-155.
4. KEKUDA, R., KARANDE, A. A. JACOB, A. N. K. AND SAVITHRI, H. S. *Virology*, 1993, 193, 959-966.
5. BUDOWSKI, E. I., SVERDOV, E. D. AND MONASTYRSKAYA, G. S. *FEBS Lett.*, 1972, 25, 201-204.
6. BONI, I. V. AND BUDOWSKY, E. I. *J. Biochem. (Tokyo)*, 1973, 73, 821-830.
7. SIMUKOVA, N. A. AND BUDOWSKY, E. I. *FEBS Lett.*, 1973, 38, 299-303.
8. ABAD-ZAPATERO, C. *et al.* *Nature*, 1980, 286, 33-39.
9. HIREMATH, C. N., MUNSHI, S. K. AND MURTHY, M. R. N. *Acta Cryst. B*, 1990, 46, 562-567.

Thesis Abstract (Ph. D.)

Organisation and structure of the gene for a 19 kD structural protein of colitis bacteriophage by M. V. Gopalakrishnan

Research supervisors: J. D. Padayatty and T. Ramasarma

Department: Biochemistry

1. Introduction

The colitis bacteriophage was isolated at the Central Drug Research Institute, Lucknow, India, in 1955. It is a lytic bacteriophage of enteric bacteria. Its morphological and immunological distinction from other known phages are well supported by nucleic-acid sequencing and structural protein analysis. It has a dsDNA genome of about 38 kb. The phage was found to have an isometric icosahedral head of about 50 nm (vertex-vertex) diameter and a long flexible tail of 100 × 100 nm which terminates in a bulbous structure by transmission electron microscopy. The phage has six structural proteins of 19 to 130 kD¹. The phage codes for two lytic enzymes^{2, 3}, both of which have been characterised in our laboratory. The genes for them were identified and one of them was sequenced. In the present study the gene for a 19-kD structural protein was sequenced. The sequence analysis and coupled transcription and translation experiments suggest that a translational frameshifting may be involved in producing the full-length 19 kD protein. A restriction enzyme map of the phage DNA was constructed. The phage genome was found to be terminally redundant and shown to possess limited circular permutation. The concatemeric phage DNA may be filled by headful packaging mechanism.

2. Experimental

The colitis bacteriophage was purified by CsCl density gradient and the structural proteins were separated by SDS-PAGE. The gene for the 19-kD coat protein was cloned and completely sequenced. The restriction enzyme digests of the phage DNA were analysed by gel electrophoresis and Southern blot hybridisation. The pBR322 carrying the lytic enzyme gene of the phage was injected in onion bulbs and the expression of the lytic enzyme was assayed using a turbidometric assay. Various restriction fragments containing this gene were used in a coupled transcription and translation system to study the expression of the coat protein gene.

2. Results and discussion

A 2.3-kb BamHI fragment carrying the 19-kD protein gene and the lytic enzyme gene was cloned in M13 vectors and sequenced. The sequence analysis revealed an open reading frame which can code for a 14-kD protein. The complete protein of 19 kD cannot be coded by any of the five other reading frames within the 680 bp Avall frag-

ment. By coupled transcription and translation it was shown to contain the complete coding requirement for the 19-kD protein. The region of termination of translation contains a stretch of A residues followed by the termination codon TGA and a stem and loop structure. All these are components of high-level frame shift signals as observed in many of the reteroviral genes⁴ and *E. coli* release factor RF2 gene. But this signal differs from the rest in being intragenic and its sequence is not similar to that of the intragenic frameshift signal in gene 10 A of T7 bacteriophage. The stemloop structure also terminates in a stretch of T residues and is a potential rho-independent termination signal. The synthesis of the 19-kD protein would require transcriptional readthrough which can be facilitated by efficient translation precluding the formation of terminating secondary structure in the messenger RNA. Sequence analysis indicated possibilities of alternative secondary structures which may have a role in transcriptional and translational regulation of the structural protein gene. The effective expression of this gene may require transcriptional and translational transgressions.

The 2.3-kb DNA fragment was mapped on to the phage genome. A restriction map of the phage genome was constructed using restriction analysis and Southern hybridization. The phage DNA was found to be terminally redundant and to have a restricted circular permutation. The 'pac' fragment which is the signal for phage DNA packaging was identified and mapped. The headful packaging mechanism, as revealed by hybridization analysis, resembles that of phage p22⁵.

The 2.3-kb BamHI insert cloned in pBR322 has a lytic enzyme gene in addition to the 19-kD structural protein gene. This lytic enzyme has 30-fold higher specific activity than egg white lysozyme on sensitized *E. coli* cells. But the lytic enzyme does not act on *Micrococcus lysodeikticus* cells unlike lysozyme. This lytic enzyme gene was used as a marker for gene transfer techniques in plant tissues. The lytic activity could be detected in germinating onion bulbs previously injected with the plasmid carrying the lytic enzyme gene⁶. The enzyme activity was not detected in bulbs injected with or without the vector DNA. Free plasmid was undetectable with or without the vector DNA. Free plasmid was undetectable in such tissues by the methods of transformation or Southern blot hybridization.

References

1. SUBRAHMANYAM, Y. V. B. K. AND PADAYATTY, J. D. *Biochem. Int.*, 1988, 16, 701.
2. GUPTA, A. AND PADAYATTY, J. D. *Biochem. Int.*, 1990, 21, 1013.
3. VASAVADA, H., MURTHY, I. AND PADAYATTY, J. D. *Gene*, 1985, 34, 9.
4. WEISS, R. B., DUNN, D. M., ATKINS, J. F. AND GESTELAND, R. F. *Cold Spring Harbor Symp. Quant. Biol.*, 1987, 52, 687.
5. BACHI, B. AND ARBER, W. *Mol. Gen. Genet.*, 1977, 153, 311.
6. GOPALAKRISHNAN, M. V. AND PADAYATTY, J. D. *Curr. Sci.*, 1990, 59, 386.

Thesis Abstract (Ph. D.)

Biochemical and immunological studies on methyl isocyanate exposure by K. S. Venkateswaran

Research supervisor: P. V. Subba Rao

Department: Biochemistry

1. Introduction

Following the release of the contents of methyl isocyanate (MIC) storage tank no. 610 from the Union Carbide India Ltd at Bhopal on December 2-3, 1984, a number of scientific investigations were initiated to understand the

acute and chronic effects of MIC exposure. The present study was aimed at establishing any evidence of the entry of MIC into the biological system, to evaluate the hypersensitivity reactions induced and the immunotoxic potential of MIC to cause any long-term effects following inhalation exposure.

2. Experimental and discussion

Hemoglobin, one of the most abundant proteins present in fairly pure form in circulation, was chosen as the candidate macromolecule to find out the formation of protein-isocyanate adduct in the blood of MIC-inhaled animals. Gas liquid chromatography¹ (GLC) and high-performance liquid chromatography (HPLC) methods were standardized for the detection of N-methyl carbamylated hemoglobin converted by cyclization into 3-methyl-5-isopropyl hydantoin. GLC analyses of blood from rats and rabbits revealed carbamylation of hemoglobin after acute inhalation exposure to MIC indicating that MIC can cross the alveolar-blood barrier to enter systemic circulation². GLC and HPLC analyses of the blood samples of the Bhopal gas victims also brought to light the presence of carbamylated hemoglobin further establishing the *in vivo* reaction of MIC with hemoglobin³.

Immunochemical techniques have been explored to study the impact of MIC exposure on the human population. The present investigation has been undertaken to assess the prolonged effects and to explain the plausible underlying mechanisms in causing the pathogenic processes in the affected persons. MIC-human serum albumin (HSA-MIC) conjugates have been synthesized and used for checking the ability of MIC to evoke specific immunological reactions. Solid-phase radioimmuno assay (SPRIA) and avidin biotin micro enzyme-linked immunosorbent assay (AB-microELISA) have been employed for monitoring the serum collected at different intervals from MIC-exposed individuals at Bhopal along with appropriate control subjects. Induction of auto-antibodies in these sera has also been evaluated. Significant elevation in either MIC-specific antibodies⁴ or alterations in the auto-antibodies level have not been noticed in the sera tested indicating that isocyanate-specific IgE antibody-mediated pulmonary hypersensitivity may not be the cause of the recurrent respiratory disorders noted at Bhopal.

A mouse model was developed to study the induction of MIC-specific IgG and IgE antibodies⁵. Immunization of Balb/c mice with HSA-MIC conjugate resulted in the production of hapten-specific IgG and IgE antibodies demonstrable by AB-microELISA and SPRIA, respectively. Even after removing the HSA-specific antibodies by adsorption with immobilized HSA, immunological reactivity of these antibodies observed with HSA conjugated to toluene diisocyanate (TDI), hexamethylene diisocyanate (HDI) and diphenylmethane diisocyanate (MDI) indicated the reaction between the antibodies and the isocyanate-altered epitopes of the carrier protein. MIC-specific antibodies purified by immunoaffinity chromatography on keyhole limpet hemocyanin-MIC-sepharose did not cross-react with the new antigenic determinants generated, presumably the isocyanate-protein bond regions of the modified carrier protein⁶. The specificity of the hapten and modified HSA-specific antibodies was established by competitive binding assays. This binding was further established using the mouse monoclonal antibodies produced by HSA-MIC immunization.

Potential of MIC to produce specific humoral immune response was evaluated following acute inhalation exposure of mice to MIC. Kinetics of antibody induction by immunization with MIC conjugated to a homologous carrier protein-mouse serum albumin- and a heterologous protein-L-132 (extract of human lung epithelial cell line proteins) was also studied. Significant levels of antibodies could not be demonstrated in mice exposed to single inhalation of MIC and low amounts of antibodies were induced only after repeated exposures. MSA-MIC was a poor sensitizer compared to L-132-MIC for the induction of MIC-specific antibodies and considerable immune response could be seen only on Day 28 after booster immunization with MSA-MIC.

Mice were exposed to 67.8, 33.9 and 19.4 mg.m⁻³ MIC in an all-glass static inhalation chamber. Immunotoxicological evaluation of these mice was performed after a follow up period of 7 and 14 days. Any significant alterations in the terminal body weights, relative organ weights of lymphoid organs, erythrocyte counts, total and differential leukocyte counts, cellularity and viability of spleen and thymus were not observed. Humoral immune response to the antigens sheep red blood cells and lipopolysaccharide was not affected as measured by the number of antibody-forming cells, hemagglutination and hemolysin titres. Cell-mediated immunity tested by delayed type hypersensitivity response to sheep red blood cell showed a transient suppression that recovered to normal level by 14 days. Lymphoproliferative responses to mitogens were not found to be affected by MIC exposure. This

investigation indicates no appreciable immunotoxic effects in mice exposed to single sub-lethal concentrations of MIC.

References

1. VENKATESWARAN, K. S. *et al.* Detection of isocyanate-induced modification of haemoglobin by gas chromatography, *J. Forensic Sci. Soc. India*, 1986, 20, 27.
2. RAMACHANDRAN, P. K. *et al.* Gas chromatographic studies on the carbamylation of haemoglobin by methyl isocyanate in rats and rabbits, *J. Chromat.*, 1988, 426, 239-246.
3. VENKATESWARAN, K. S. *et al.* Monitoring of haemoglobin-methyl isocyanate adduct using diode array detector by high performance liquid chromatography, *Biochem. Int.*, 1992, 28, 745-750.
4. VENKATESWARAN, K. S. *et al.* Evaluation of antibodies in the serum of methyl isocyanate exposed Bhopal population, *Proc. 6th Int. Cong. Immunol.*, 1986, 5.43, p. 44.
5. NAZIRUDDIN, B. *et al.* MIC-specific antibody response in Balb/c mice, *NER Allergy Proc.*, 1988, 9, 547.
6. VENKATESWARAN, K. S. *et al.* Induction of antibodies to new antigenic determinants in mice by isocyanate-human serum albumin sensitization, *Proc. XIX A. Conf. Indian Immunol. Soc.*, 1993, pp. 18-19.

Thesis Abstract (Ph. D.)

3, 5-Dichlorocatechol 1, 2-dioxygenase: Purification, characterization, expression and nucleotide sequence of its gene from *Pseudomonas cepacia* CSV90 by Manzoor Ahmad Bhat

Research supervisors: N. Appaji Rao and C. S. Vaidyanathan

Department: Biochemistry

1. Introduction

Microorganisms in nature have apparently evolved the ability to degrade many toxic and recalcitrant aromatic compounds, which reach our environment as industrial effluents, sewage, pollutants and secondary metabolites¹. Structural plasticity of the genetic machinery of the microbes endows them with a degradative capability that can be quickly adapted in response to substrate variability. Such expanding catabolic versatilities may reveal principles not yet encountered in the intensively studied metabolic pathways. The toxic mutagenic and carcinogenic effects of various chlorinated compounds make studies of these compounds at various levels extremely important.

2, 4-Dichlorophenoxyacetic acid (2, 4-D), commonly used as a herbicide, was chosen as a model compound to understand the biochemical and genetic basis of its metabolism in *Pseudomonas cepacia*.

We have previously reported the purification and characterization of 2, 4-dichlorophenol hydroxylase, a flavoprotein monooxygenase catalyzing the conversion of 2, 4-dichlorophenol to 3, 5-dichlorocatechol². No information was available regarding the fate of 3, 5-dichlorocatechol. The catechol ring cleavage in aromatic metabolism is very crucial to convert aromatic compounds into aliphatic ones, which after subsequent reactions are then funneled into tricarboxylic acid cycle.

The aim of the present study was to understand the nature of 3, 5-dichlorocatechol dioxygenase reaction, the genetic basis of 2, 4-D degradation and determining the nucleotide sequence of 3, 5-dichlorocatechol dioxygenase gene in *Pseudomonas cepacia* CSV90.

Table I
Molecular and kinetic properties of 3, 5-dichloro-
catechol 1, 2-dioxygenase

Molecular weight of native enzyme	
HPLC-LS-RI method	56,000
Gel filtration	66,000
Molecular weight of subunit	
Gel filtration in 6 M guanidine-HCl	29,000
SDS-PAGE	31,000
Subunit composition	α_2
Iron content (mol/mol enzyme)	0.89
Kinetic properties at 25°C and pH 8.0	
Specific activity (μ mol/ min/ mg)	11.1
$K_{cat} s^{-1}$	34.7
K_m for 3, 5-dichlorocatechol	4.4
K_m for oxygen	652

2. Materials and methods

A new strain of *Pseudomonas cepacia* designated as *Pseudomonas cepacia* CSV90 was used for this study. The strain CSV90 was cultured in basal salts medium, pH 7.2 containing 0.2% 2, 4-D as the sole source of carbon and energy. The metabolic intermediates were identified by gas chromatography and mass spectrometry. A procedure was developed for the synthesis of the substrate 3, 5-dichlorocatechol. The enzyme 3, 5-dichlorocatechol was purified using DEAE-sephacel, phenyl-sepharose and gel filtration chromatography.

For the identification of any plasmid in the strain CSV90, a modified procedure from that of Kado and Liu³ was developed. For curing of the strain CSV90, electro-transformation of the cured derivative (*Pseudomonas cepacia* MAB1), transposon mutagenesis, and recombinant DNA techniques, established procedures were used. DNA sequencing was performed according to the chain termination method using fluorescent dye-labeled primers on an automated DNA sequencing system, Applied Biosystems Model 373A. The nucleotide sequences were analyzed using software packages developed by Genetyx Computer Group (GCG), University of Wisconsin, Madison, USA.

3. Results and discussion

The strain of *Pseudomonas* isolated in our laboratory was identified as *Pseudomonas cepacia*. We designated this isolate as *Pseudomonas cepacia* strain CSV90 because previously reported isolates of *P. cepacia* were 2, 4-D nondegrading.

The analysis of the synthesized compound by NMR and IR spectroscopy, mass spectrometry and elemental analysis revealed a compound which had characteristics like 3, 5-dichlorocatechol. This compound was efficiently used as substrate by 3, 5-dichlorocatechol 1, 2-dioxygenase confirming its identity⁴. The induction profile of 2, 4-dichlorophenol hydroxylase and 3, 5-dichlorocatechol dioxygenase showed that both were maximally induced between 22 and 24 h. The purification of 3,5-dichlorocatechol dioxygenase yielded an enzyme preparation which showed single bands on the non-denaturing and denaturing polyacrylamide gel electrophoresis. The native molecular weight of the enzyme was estimated to be 56,000 and a subunit molecular weight was estimated to be 29,000, suggesting that the purified enzyme was homogeneous and consists of two identical subunits, *i. e.*, a homodimer. During the automated Edman degradation of the enzyme up to 44 residues, a single amino acid was released at each step, suggesting that the enzyme is composed of two identical subunits, supporting our gel filtration data⁴. The iron content was determined to be 0.89 mol per mole of enzyme. The enzyme showed a broad absorption spectrum with a maximum at about 425 nm in the visible region. When the enzyme was treated with sodium

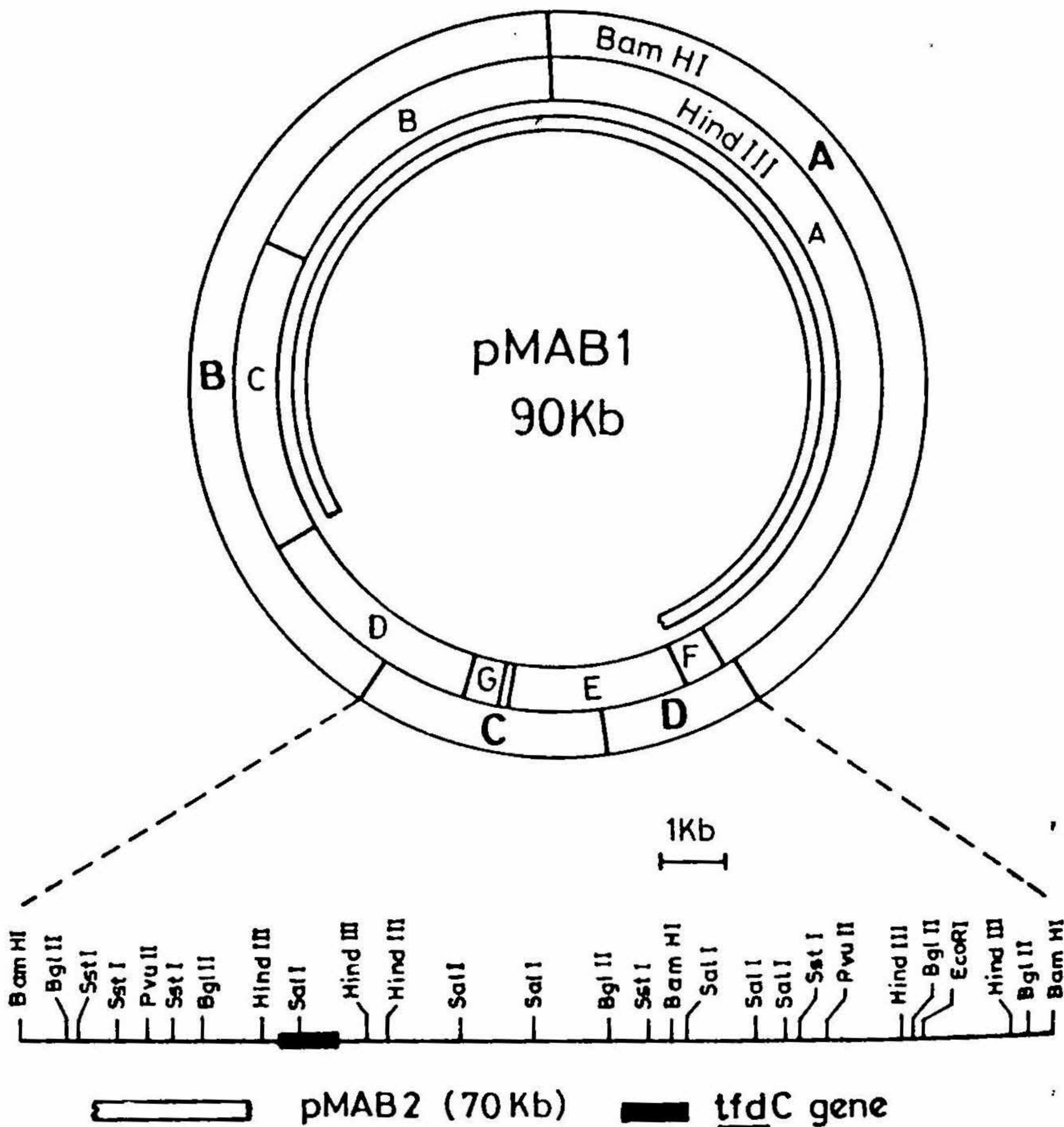


FIG. 1. Physical map of the plasmid, pMAB1 from *Pseudomonas cepacia* CSV90. A detailed restriction map of the BamHI 10 kb and 6 kb fragments which were found to be deleted in pMAB2 is shown. The broken circle inside represents the approximate size of pMAB2. Black bar indicates the location of 3, 5-dichlorocatechol 1, 2-dioxygenase (*tfdC*) gene.

dithionite, the visible absorption almost disappeared, and reappeared again after aeration, suggesting that the iron in the enzyme is in the ferric state. When the organic substrate, 3, 5-dichlorocatechol was added to the enzyme under anaerobic conditions, an immediate change of color from deep red to purple was observed and the absorption spectrum revealed a large red shift. Initial velocity studies of the enzyme were carried out as functions of 3, 5-dichlorocatechol and oxygen concentrations, and K_m values obtained for 3, 5-dichlorocatechol and oxygen were 4.4 and 652 μM , respectively. To examine the substrate specificity, catechol derivatives substituted at different positions were used as substrates. All the spectra of the products formed and their molar absorption coefficients

were in good agreement with those of muconic acid derivatives, respectively. That is, no extradiol-cleaving activity was observed with any of the catechol derivatives. Using an air-saturated tris-HCl buffer (pH 8.0), the apparent values of K_m and V_{max} were obtained from $[S]/V$ vs $[S]$ plots and specificity constants (k_{cat}/k_m) were calculated. Chlorocatechols were good substrates and 3, 5-dichlorocatechol had the highest specificity constant of $7.3 \mu\text{M}^{-1}\text{s}^{-1}$. The molecular and kinetic properties of 3, 5-dichlorocatechol 1, 2-dioxygenase are given in Table I.

The strain CSV90 could grow on 2, 4-D up to a concentration of 0.25% as a sole source of carbon. This strain could not grow on L broth containing $5 \mu\text{g/ml}$ HgCl_2 , and failed to utilize 3-chlorobenzoate, but was able to grow on 2-methyl-4-chlorophenoxyacetate when used as the sole carbon source. These characteristics are different from that of *Alcaligenes eutrophus* JMP134 in terms of HgCl_2 resistance and 3-chlorobenzoate utilization⁵. The strain CSV90 was found to harbor a high molecular weight plasmid designated as pMAB1⁶.

In the case of *A. eutrophus* JMP134 harboring the plasmid pJP4 2, 4-D degradation and HgCl_2 resistance have been shown to be plasmid coded. The ability of the strain CSV90 to grow on 2, 4-D agar was very unstable and lost irreversibly. Many cured derivatives of the strain CSV90 were obtained after spontaneous curing on L agar plates, i.e., these derivatives failed to grow on 2, 4-D and showed complete loss of the plasmid pMAB1 (e.g., *Pseudomonas cepacia* MAB1) or carried a smaller plasmid than pMAB1 designated as pMAB2 (e.g., *Pseudomonas cepacia* MAB2). Treatment of the strain CSV90 with a curing agent, mitomycin C resulted in generation of 2, 4-D-negative segregants with the frequency of 20–50%. In such derivatives, no plasmid was detected corresponding to pMAB1 or pMAB2. The strain MAB1 was transformed with purified pMAB1 by electroporation, which enabled this strain to grow normally on 2, 4-D agar plates like CSV90 and a similar plasmid like pMAB1 was recovered from the transformants, thus confirming the involvement of the plasmid, pMAB1 in 2, 4-D degradation.

The physical maps of the plasmids pMAB1 and pMAB2 were constructed by single and double digestion with BamHI and HindIII, and various fragments were cloned to obtain more precise maps⁶ as shown in Fig. 1. The restriction analysis of plasmids pMAB1 and pMAB2 revealed that a portion sized approximately 20-kilobase (kb) had been deleted from pMAB1 with the loss of 2, 4-D degrading ability. The molecular sizes of the plasmids pMAB1 and pMAB2 have been estimated to be 90 and 70 kb, respectively. The physical map of pMAB1 was different from that of pJP4⁵. The plasmid pMAB1 was digested with BamHI and HindIII; the resulting fragments were subcloned and separately analyzed for dioxygenase activity. Except for plasmid pMAB786 which showed high levels of activity for *tfdc* gene product, no other activities could be observed. Cells carrying pMAB7860, a plasmid containing the same 1.6-kb HindIII insert as in pMAB786 but in opposite orientation with respect to the vector promoter, did not produce the enzyme. Therefore, the expression of *tfdc* in pMAB786 was due to a read-through transcription from the vector promoter. The enzyme activity of *tfdc* product was not observed in the absence of IPTG, ruling out constitutive expression. The nucleotide sequence of the 1.6-kb HindIII fragment and the deduced amino acid sequence of the *tfdc* gene product indicated an open reading frame starting from nucleotide 337 to 1101 which is capable of specifying 255 amino acids with the predicted molecular weight of 28,300. This was in good agreement with the determined molecular weight established by various physical methods. The amino acid sequence and composition determined from the purified enzyme was in perfect agreement with that deduced from the DNA sequence. This agreement established that this is indeed the sequence of *tfdc*, the structural gene for 3, 5-dichlorocatechol 1, 2-dioxygenase⁶. Several bases upstream from the initiation codon was found a typical Shine-Dalgarno sequence, GGAGGCA and putative *Pseudomonas* promoter-like sequences. The dioxygenase gene (*tfdc*) was cloned in an expression vector pKK223-3 and the recombinant plasmid, pMAB1963 produced the dioxygenase enzyme up to 6% of the total soluble protein after IPTG induction.

References

- SCHNEIDER, M. H. *Persistent poisons: Chemical pollutants in the environment*, New York Academy of Sciences, New York, 1979.
- RADJENDIRANE, V., BHAT, M. A. AND VAIDYANATHAN, C. S. *Arch. Biochem. Biophys.*, 1991, 288, 169–176.
- KADO, C. I. AND LIU, S. T-. *J. Bacteriol.*, 1981, 145, 1365–1373.
- BHAT, M. A. *et al.* *Arch. Biochem. Biophys.*, 1993, 300, 738–746.

5. PERKINS, E. J., GORDON, M. P.,
CACERES, O. AND LURQUIN, P. F.

J. Bacteriol., 1990, **172**, 2351–2359.

6. BHAT, M. A. *et al.*

Appl. Environ. Microbiol., 1994, **60**, 307–312.